

**COMPARATIVE STUDY OF PROPORTIONAL  
INTEGRAL (PI) AND PROPORTIONAL RESONANT (PR)  
CURRENT CONTROLLER FOR SINGLE PHASE  
INVERTER**

**MOHAMMAD PARVEZ**

**DISSERTATION SUBMITTED IN FULFILMENT OF THE  
REQUIREMENTS FOR THE DEGREE OF MASTER OF  
PHILOSOPHY**

**INSTITUTE OF GRADUATE STUDIES  
UNIVERSITY OF MALAYA  
KUALA LUMPUR**

**2017**

**UNIVERSITI MALAYA**  
**ORIGINAL LITERARY WORK DECLARATION**

Name of the candidate: **Mohammad Parvez**

Registration/Matric No: **HGF130003**

Name of the Degree: **Master of Philosophy**

Title of Project Paper/Research Report/Dissertation/Thesis (This Work): **Comparative Study of Proportional Integral (PI) and Proportional Resonant (PR) Current Controller for Single-Phase Inverter**

Field of Study: **Electrical Engineering (Control System)**

I do solemnly and sincerely declare that:

- (1) I am the sole author/writer of this work;
- (2) This work is original;
- (3) Any use of my work in which copyright exists was done by way of fair dealing and for permitted purposes and any excerpt or extract from, or reference to or reproduction of any copyright work has been disclosed expressly and sufficiently and the title of the work and its authorship have been acknowledged in this work;
- (4) I do not have any actual knowledge nor do I ought to reasonably to know that the making of this work constitutes an infringement of any copyright work;
- (5) I hereby assign all and every rights in the copyright to this work to the University of Malaya ("UM"), who henceforth shall be owner of the copyright in this work and that any reproduction or use in any form or by any means whatsoever is prohibited without the written consent of UM having been first had and obtained;
- (6) I am fully aware that if in the course of making these works I have infringe any copyright whether intentionally or otherwise, I may be subject to legal action or any other action as may be determined by UM.

Candidate's Signature

Date

Subscribe and solemnly declare before,

Witness Signature

Date

Name :

Designation :

## ABSTRACT

This research work focuses on the comprehensive analysis of proportional resonant (PR) controller for single-phase inverter. There is an increasing requirement for current-controlled voltage source inverters with very low or zero steady-state error, better transient response and lower total harmonic distortion (THD). The most promising type of current regulator for single-phase inverter is PR controller because it can introduce an infinite gain at a selected resonance frequency such as the fundamental frequency to eliminate the steady-state error, which cannot be achieved by the well-known proportional integral (PI) controller. The PI controller faces problem in both steady-state magnitude error and phase error. In addition, it also has limited disturbance rejection capability, unlike the PR controller, which can also compensate the low-order harmonics. The imperfection in current control scheme results in higher harmonic distortion of the output current. This research presents detail analysis and implementation of PR current controller in single-phase inverter applications such as stand-alone and grid-connected renewable energy systems, energy storage systems and backup power supplies. Thus, the mathematical model of PR controller has been analyzed. In order to realize the important control features over conventional PI controller, PI controller has also been implemented in the same inverter and mathematically analyzed. The performances for both of these controllers have been analyzed in terms of steady-state and transient responses and current harmonics level. The effects of frequency variation on the PR controller performance have also been shown. The experimental result shows that the PR controller achieves zero steady-state error, better transient response and reduces the low-order harmonics distortion of the output current compared to PI controller. The harmonics has further been reduced by incorporating selective harmonic compensation with PR controller. The performances of the implemented controllers are simulated and compared in the widely used software

such as the MATLAB/Simulink environment which has reduced the developmental time and cost of the switching system. The experimental results of a 250 W laboratory test set have been implemented to validate the theoretical analysis and control principles of the PR and PI controllers.

University of Malaya

## ABSTRAK

Kerja penyelidikan ini memberi tumpuan kepada analisis pengawal berkadar salunan (PR) bagi penyongsang fasa tunggal. Terdapat keperluan yang semakin meningkat bagi penyongsang sumber voltan kawalan arus dengan ralat yang sangat rendah atau ralat sifar pada keadaan mantap, sambutan fana yang lebih baik dan herotan harmonik (THD) yang rendah. Jenis kawalan arus yang paling baik untuk penyongsang fasa tunggal adalah pengawal PR kerana ia boleh memperkenalkan gandaan tidak terhingga pada frekuensi salunan terpilih seperti frekuensi asas untuk menghapuskan ralat keadaan mantap yang tidak boleh dicapai oleh pengawal berkadar kamiran (PI). Pengawal PI menghadapi masalah dalam keadaan mantap dan kesilapan dari segi magnitud dan fasa. Di samping itu, ia juga mempunyai keupayaan penolakan gangguan terhad, tidak seperti pengawal PR yang boleh memberi pampasan kepada harmonik susunan rendah. Ketidaktepatan dalam skim kawalan menyebabkan herotan harmonik yang lebih tinggi pada arus keluaran. Kajian ini membentangkan analisis yang terperinci dan pelaksanaan kawalan salunan PR dalam aplikasi penyongsang fasa tunggal seperti sistem tenaga boleh diperbaharui yang berdiri sendiri dan tersambung grid, sistem penyimpanan tenaga dan bekalan kuasa sandaran. Oleh itu, model matematik pengawal PR telah dianalisa. Dalam usaha untuk menunjukkan kelebihan atau ciri-ciri penting bagi kawalan PR, pengawal PI juga telah dilaksanakan pada penyongsang yang sama untuk perbandingan. Prestasi untuk kedua-dua pengawal ini telah dianalisa dari segi tindak balas keadaan mantap, keadaan fana, dan tahap harmonik arus. Kesan perubahan frekuensi keatas prestasi pengawal juga telah terbukti. Hasil eksperimen menunjukkan bahawa pengawal PR mencapai ralat sifar pada keadaan mantap, sambutan fana yang lebih baik dan herotan harmonik arus yang rendah berbanding pengawal PI. Harmonik boleh dikurangkan lagi dengan menggabungkan pampasan harmonik terpilih dengan pengawal PR. Prestasi pengawal juga dilaksanakan secara simulasi dan dibandingkan

dengan perisian MATLAB/ Simulink. Keputusan eksperimen yang diperolehi daripada set ujian makmal 250W telah mengesahkan analisis dan teori kawalan arus PR dan PI.

University of Malaya

## ACKNOWLEDGEMENTS

First of all, I am really grateful to Allah in blessing me with the knowledge, giving me the courage to tackle all problems and helping me in every step of my life.

I would like to express my deepest appreciation and gratitude to my supervisor, **Professor Dr. Nasrudin Bin Abd Rahim** for motivating and guiding me during my thesis work. It has been a pleasure to collaborate with him and I hope to continue. His wise experience in the field of electrical power engineering has enlightened me throughout the project.

I would like to express my indebted gratitude to my supervisor, **Dr. Mohamad Fathi Bin Mohamad Elias** for his outstanding support, contribution and invaluable assistance in the achievement and development of my MPhil thesis.

I am greatly indebted to my father, mother, wife, daughter and elder brother for their continuous loving support, inspiration and encouragement.

I also express my gratitude to all UMPEDAC staff for helping me directly or indirectly to carry out my research work. I gratefully acknowledge the privileges and opportunities offered by the University of Malaya.

## TABLE OF CONTENTS

ORIGINAL LITERARY WORK DECLARATION .....	ii
ABSTRACT .....	iii
ABSTRAK .....	v
ACKNOWLEDGEMENTS .....	vii
TABLE OF CONTENTS .....	viii
LIST OF FIGURES .....	xi
LIST OF TABLES .....	xiv
LIST OF SYMBOLS AND ABBREVIATIONS .....	xv
<b>CHAPTER 1: INTRODUCTION .....</b>	<b>1</b>
1.1 Background .....	1
1.2 Problem Statement .....	4
1.3 Research Objectives .....	4
1.4 Methodology .....	5
1.5 Scope of Research .....	6
1.6 Thesis Outline .....	7
<b>CHAPTER 2: AN OVERVIEW OF CURRENT CONTROL TECHNIQUES .....</b>	<b>8</b>
2.1 Introduction .....	8
2.1.1 Current Control Structures for Single-Phase Inverter .....	8
2.1.2 Linear Current Control for Single-Phase Inverters .....	9
2.1.2.1 Proportional-integral (PI) controller .....	9
2.1.2.2 Proportional-resonant (PR) controller .....	10



2.1.2.3 Repetitive current (RC) controller .....	12
2.1.3 Nonlinear Current Control for Single-Phase Inverters.....	13
2.1.3.1 Dead-beat (DB) controller.....	13
2.1.3.2 Hysteresis controller.....	14
2.1.3.3 Predictive controller .....	16
2.1.4 Analysis of Current Control Structures.....	16
2.1.5 Current Harmonics Compensation.....	17
2.1.5.1 Harmonics compensation using PI controllers.....	17
2.1.5.2 Harmonics compensation using PR controllers .....	18
2.1.5.3 Harmonics compensation using nonlinear controllers .....	21
2.2 Summary.....	21
 <b>CHAPTER 3: ANALYSIS AND IMPLEMENTATION OF PI AND PR</b>	
<b>CURRENT CONTROLLERS .....</b>	
<b>22</b>	
3.1 Introduction.....	22
3.2 Single-Phase PWM Inverter.....	22
3.3 Current Control Scheme for Single-Phase Inverter with LC-Filter .....	23
3.3.1 Analysis the Design of Filter Parameters.....	25
3.3.2 Analysis the Design of PR Current Controller.....	27
3.3.2.1 Frequency response of open-loop non-ideal PR controller.....	27
3.3.2.2 Frequency response of closed-loop control system .....	30
3.4 Implementation of PI Controller Using Discrete Transfer Function .....	33
3.5 Implementation of PR Controller Using Discrete Transfer Function .....	34
3.6 Experimental Design and Setup .....	36

3.7 Summary.....	38
<b>CHAPTER 4: RESULTS AND DISCUSSION .....</b>	<b>39</b>
4.1 Introduction.....	39
4.2 Steady-State Response of PI Controller.....	39
4.3 Steady-State Response of PR Controller.....	42
4.4 Transient Response of PI Controller.....	45
4.5 Transient Response of PR Controller.....	47
4.6 Effect of Frequency Variation.....	50
4.7 Summary Comparison of Current Controllers.....	52
<b>CHAPTER 5: CONCLUSION AND FUTURE WORK .....</b>	<b>53</b>
5.1 Conclusion .....	53
5.2 Future Work .....	53
REFERENCES.....	54
LIST OF PUBLICATIONS .....	61

## LIST OF FIGURES

Figure 1.1: Average annual growth rates of renewable energy capacities.....	1
Figure 1.2: Installed capacity in the world by end of 2014, (a) wind energy and (b) solar/PV energy .....	2
Figure 1.3: Installed capacity in the world by the top ten countries in 2014, (a) wind energy and (b) solar/PV energy.....	2
Figure 1.4: Flowchart of research methodology.....	6
Figure 2.1: Structure of renewable power generation system with different energy sources .....	9
Figure 2.2: General current control structure for $dq$ -control strategy.....	9
Figure 2.3: General current control structure for $\alpha\beta$ -control strategy.....	10
Figure 2.4: Frequency response (a) ideal PR controller; and (b) non-ideal PR controller; using $K_p=1$ , $K_i=20$ , $\omega_o=314$ rad/s and $\omega_c=10$ rad/s .....	11
Figure 2.5: Block diagram of RC current controller .....	12
Figure 2.6: Block diagram of dead-beat controller .....	14
Figure 2.7: Configuration of hysteresis current controller.....	15
Figure 2.8: Hysteresis current controller operational waveform .....	15
Figure 2.9: Block diagram of predictive controller.....	16
Figure 2.10: Block representation of harmonic compensator with PR controller.....	18
Figure 2.11: Bode diagram of HC for the individual of 3 <sup>rd</sup> , 5 <sup>th</sup> and 7 <sup>th</sup> harmonic with $K_{ih}=1$ , $\omega_c=1$ rad/s and $\omega_o=314$ rad/s .....	20
Figure 2.12: Bode diagram of HC for the summation of 3 <sup>rd</sup> , 5 <sup>th</sup> and 7 <sup>th</sup> harmonics with $K_{ih}=1$ , $\omega_c=1$ rad/s, $\omega_c=10$ rad/s and $\omega_o=314$ rad/s.....	20
Figure 2.13: Bode diagram of PR+HC using $K_{ih}=1$ , $\omega_c=1$ rad/s, $\omega_c=10$ rad/s and $\omega_o=314$ rad/s.....	21

Figure 3.1: Schematic diagram of a single-phase inverter.....	22
Figure 3.2: Inverter supplying power to load through the LC-filter. ....	23
Figure 3.3: Block diagram of a current control scheme for single-phase inverter with LC-filter.....	24
Figure 3.4: Equivalent circuit of an LC-filter. ....	25
Figure 3.5: Frequency response of LC filter with $L = 5$ mH and $C = 0.22$ $\mu$ F.....	26
Figure 3.6: Frequency of the non-ideal PR controller as a function of (a) $K_i$ changes, (b) $\omega_c$ changes and (c) $K_p$ changes. ....	28
Figure 3.7: Bode plot of open-loop non-ideal PR controller ( $K_p = 0.5$ , $K_i = 1000$ and $\omega_c =$ $0.1$ rad/s).....	30
Figure 3.8: Block diagram of closed-loop current control scheme.....	30
Figure 3.9: Frequency response of closed-loop transfer function using PI controller ( $K_p$ $= 0.5$ and $K_i = 200$ ). ....	32
Figure 3.10: Frequency response of closed-loop transfer function using PR controller ( $K_p = 0.5$ , $K_i = 1000$ , $\omega_0 = 314$ rad/s and $\omega_c = 0.1$ rad/s).....	32
Figure 3.11: Block diagram of experimental design.....	36
Figure 3.12: Prototype setup of the single-phase inverter using resistive load (a) Front view and (b) Top view.....	37
Figure 4.1: Simulation results using PI controller (a) load current, (b) load voltage and (c) FFT analysis.....	40
Figure 4.2: Experiment results using PI controller ( $K_p = 0.5$ and $K_i = 200$ ) (a) load current and (b) load voltage. ....	41
Figure 4.3: Experiment result using PI controller showing load current harmonics. ....	41
Figure 4.4: Experiment results using by the PI controller ( $K_p = 0.7$ and $K_i = 200$ ) (a) load current and (b) load voltage. ....	42

Figure 4.5: Simulation results using PR controller (a) load current, (b) load voltage and (c) FFT analysis.....	43
Figure 4.6: Experimental results using PR controller ( $K_p = 0.5$ and $K_i = 1000$ ) (a) load current (b) load voltage .....	44
Figure 4.7: Experimental results using PR controller showing load current harmonics.	44
Figure 4.8: Simulation result showing the transient response in load current by using the PI controller.....	45
Figure 4.9: Experimental results showing transient response using PI controller for $K_p = 0.5$ , $K_i = 100$ .....	46
Figure 4.10: Experimental results showing transient response using PI controller for $K_p = 0.5$ , $K_i = 200$ .....	46
Figure 4.11: Experimental results showing transient response using PI controller for $K_p = 0.5$ , $K_i = 300$ .....	47
Figure 4.12: Simulation result-transient response of load current using by the PR controller.....	47
Figure 4.13: Experiment results showing transient response using PR controller for $K_p = 0.5$ , $K_i = 1000$ .....	48
Figure 4.14: Experiment results showing transient response using PR controller for $K_p = 0.5$ , $K_i = 2000$ .....	49
Figure 4.15: Experiment results showing transient response using PR controller for $K_p = 0.5$ , $K_i = 3000$ .....	49
Figure 4.16: Effect of frequency variation using PR controller (a) under frequency at $f = 45$ Hz, (b) normal frequency at $f = 50$ Hz and (c) over frequency at $f = 55$ Hz). .....	51

## LIST OF TABLES

Table 3.1: Inverter specifications.....	38
Table 4.1: Benefits and limitations of PI and PR current controllers .....	52

University of Malaya

## LIST OF SYMBOLS AND ABBREVIATIONS

PV	: Photovoltaic
RPGS	: Renewable power generation system
PI	: Proportional integral
PR	: Proportional resonant
$K_p$	: Proportional gain constant
$K_i$	: Integral gain constant
$\omega_o$	: Fundamental frequency
$\omega_c$	: Cut-off frequency
$K_{ih}$	: Specific resonant gain
$h$	: Harmonic number
HC	: Harmonic compensator
RC	: Repetitive controller
$K_{rc}$	: Repetitive controller constant
$T_0$	: Initial time period
$T$	: Time period of phase-lead compensation
$T_s$	: Sampling time
$f_s$	: Switching frequency
$f_g$	: Grid frequency
$N$	: Signal frequency ratio
$Q(s)$	: Low pass filter
DB	: Dead-beat
$R_T$	: Equivalent internal resistance
$L_T$	: Equivalent internal inductance
$I_{ref}$	: Reference current
$I_{actual}$	: Actual current
$e$	: Error signal

$e_{min}$	: Minimum error signal
$e_{max}$	: Maximum error signal
IEC	: International Electro-technical Commission
$L_f$	: Filter inductor
$C_f$	: Filter capacitor
$r_f$	: Internal resistance of filter inductor
$R_L$	: Load resistor
$V_{inv}$	: Inverter output voltage
$V_{out}$	: Output voltage
$V_{dc}$	: DC voltage
$f_{res}$	: Resonance frequency
$I_L$	: Load current
$V_L$	: Load voltage
$V_i^*$	: Inverter reference voltage
FFT	: Fast Fourier transforms
THD	: Total harmonic distortion
DSP	: Digital signal processor
APF	: Active power filter
MPPT	: Maximum power point tracking
DC	: Direct current
AC	: Alternating current
VSI	: Voltage source inverter
ADC	: Analog to digital converter
IGBT	: Insulated-gate bipolar transistor



## CHAPTER 1: INTRODUCTION

### 1.1 Background

Global energy demand is rapidly growing and therefore meeting the future energy demand becomes a major concern worldwide. To meet the energy demand, fossil fuels which have been used since many years ago are typically used as the primary energy sources. However, fossil fuels emit greenhouse gases that highly affect the environment and humanity (Cao, 2014; Du et al., 2013; Hasanuzzaman et al., 2012; Hasanuzzaman et al., 2011; Hosseini & Abdul Wahid, 2014; Islam et al., 2014; Ünal et al., 2015; Yang et al., 2001; Yu et al., 2010).

For this reason, the alternative sources of renewable energy such as solar, wind, hydro, biomass and geothermal are getting popular. Figure 1.1 shows the average annual growth rates of renewable energy capacities in the world between 2009 and 2014. A total amount of around 370-GW wind power and 177-GW solar/PV power have been installed in the world by the end of 2014, as shown in Figure 1.2 (a) and (b) respectively. Figure 1.3 shows the total installed capacity worldwide by the top ten countries in 2014.

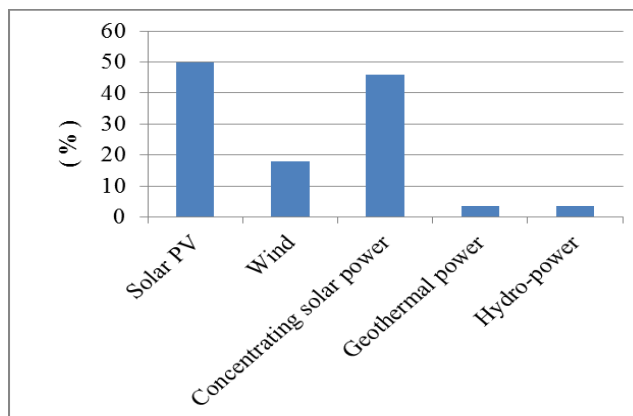
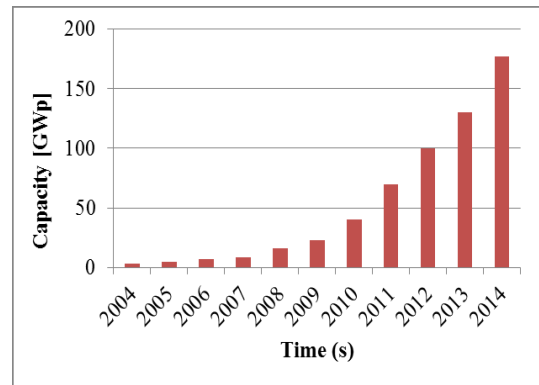
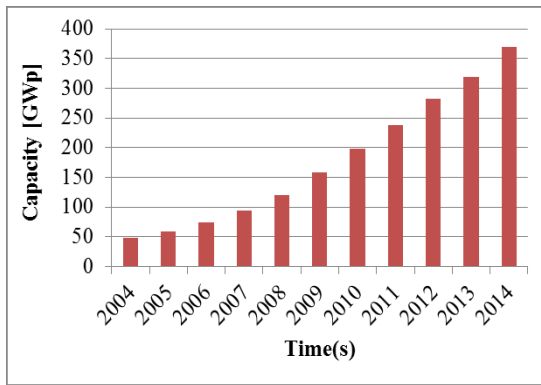


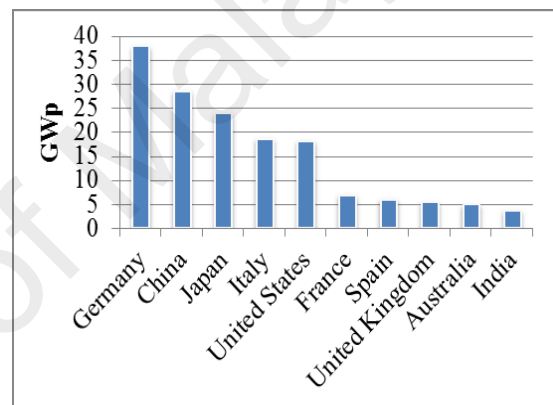
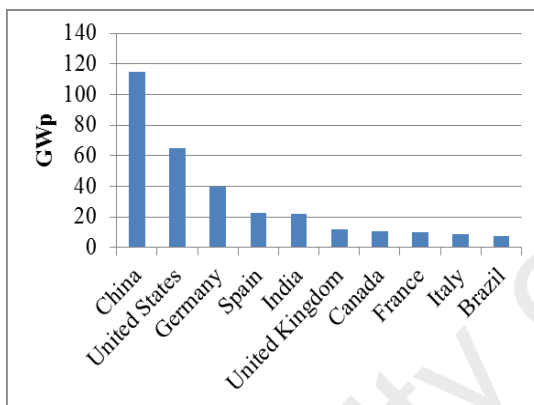
**Figure 1.1:** Average annual growth rates of renewable energy capacities (IEA, Global Energy Trends, 2014)



(a)

(b)

**Figure 1.2:** Installed capacity in the world by end of 2014, (a) wind energy and (b) solar/PV energy (IEA, Global Energy Trends, 2014)



(a)

(b)

**Figure 1.3:** Installed capacity in the world by the top ten countries in 2014, (a) wind energy and (b) solar/PV energy (IEA, Global Energy Trends, 2014)

Hence, development of power converters for renewable energy sources is becoming more and more essential to provide clean power generation. For instance, in grid-connected application, the power converter must satisfy standard performance requirements on grid parameters such as voltage, current, frequency, harmonics, power factor and flicker (IEC 61727, IEEE 1547 and VDE V 0126) . For standalone renewable energy applications, the standard on safety is available such as IEC 62109 which is also applicable to grid-connected applications. Since the standalone application is isolated from the power grid, there is no specific requirement on the performance but it is recommended that it complies the basic harmonics standard for instance as specified by

IEC 61000-3-2 or IEEE 519. With today's advancements in power electronics, inverter has becoming very common to power up ac loads used in residential and industrial sectors. The inverter is able to produce a sinusoidal output voltage and current which is important to achieve high energy efficiency and high power quality (Alepuz et al., 2006; Chung, 2000; Du et al., 2013; Hosseini & Abdul Wahid, 2014; Negroni et al., 2005; Tajuddin et al., 2015). Maintaining sinusoidal output requires voltage or current regulation to be incorporated into the inverter system, thus keeping the system output with low harmonics content for sustaining its performance, stability and reliability. The presence of harmonics reduces power quality and causes extra power losses that directly contribute to components failure and decreasing equipment's lifetime.

This study is associated with the inverter development focusing on the current control technique for single-phase inverter systems. First, an overview of various current control structures and related power quality issues that affect its performance such as current harmonics is presented. The current control structures are classified into linear and non-linear control techniques. Among the control techniques, two of them have been selected for comparison in terms of performance which are proportional integral (PI) and proportional resonant (PR), taking into account their significance and also practical implementation. In general, PI controller has been employed in many power converters applications, such as active power filters (APFs), wind turbines, water turbines, photovoltaic inverters, uninterruptable power supplies, dynamic voltage restorer, active rectifiers, boost converters, induction drives, fuel-cell inverters and micro grids. Recently, PR controller is gaining popularity because of its capability in tracking a sinusoidal reference with zero steady-state error especially for single-phase system. It can also be applied in three-phase system particularly for controlling parameters in the stationary  $\alpha\beta$ -reference frame. Simulation studies are conducted on

both PR and PI controllers using MATLAB Simulink software. A prototype of an inverter with sensor circuits was built for experimental verification of both controllers.

## **1.2 Problem Statement**

The conventional proportional integral (PI) controller is very well known and has a very good performance in various control system applications. However, when the controller is used for current control in a single-phase inverter application, it creates steady-state magnitude and phase errors especially when tracking a sinusoidal reference. A different type of controller that able to overcome these problems is called proportional resonant (PR) controller. In order to show the advantages of PR controller over the conventional PI controller, a comparative study and analysis of these controllers are performed. This study includes the design, modeling, simulation and experimental tests on a single-phase inverter prototype.

## **1.3 Research Objectives**

The objectives of this study are as follow:

1. To develop the mathematical model of PR and PI controllers.
2. To simulate current control of single-phase inverter by using PR and PI controllers in MATLAB/Simulink.
3. To build an inverter prototype with sensor circuits for experimental verification of the PR and PI controllers.
4. To evaluate the performance of both controllers in terms of current's total harmonic distortion, steady-state and transient conditions.

## 1.4 Methodology

Below are the descriptions of research methodology adopted in this study. The flowchart of research methodology is shown in Figure 1.4.

- **Literature Survey and Concept Development**

An extensive literature reviews from thesis, books, journal articles, magazines, reports and conference proceedings will be carried out to determine the latest developments in current control techniques for inverters.

- **Modeling and Simulation**

Based on literature reviews, two current controllers PI and PR will be modeled mathematically for single-phase standalone PV inverter system. The overall system will be simulated using MATLAB Simulink. The performance of the controllers will be simulated at various operating conditions.

- **Software and Hardware Development**

When the simulation results are satisfactorily, the controllers will be implemented in hardware using C programming language. The hardware is developed for verification of the controller's performance experimentally. The component will be properly selected to meet all requirements in terms of power, voltage, current and frequency.

- **Testing and Data Analysis**

The controllers will be tested at several operating conditions including steady-state and transient. The experimental results will be compared with the simulation results for verification.

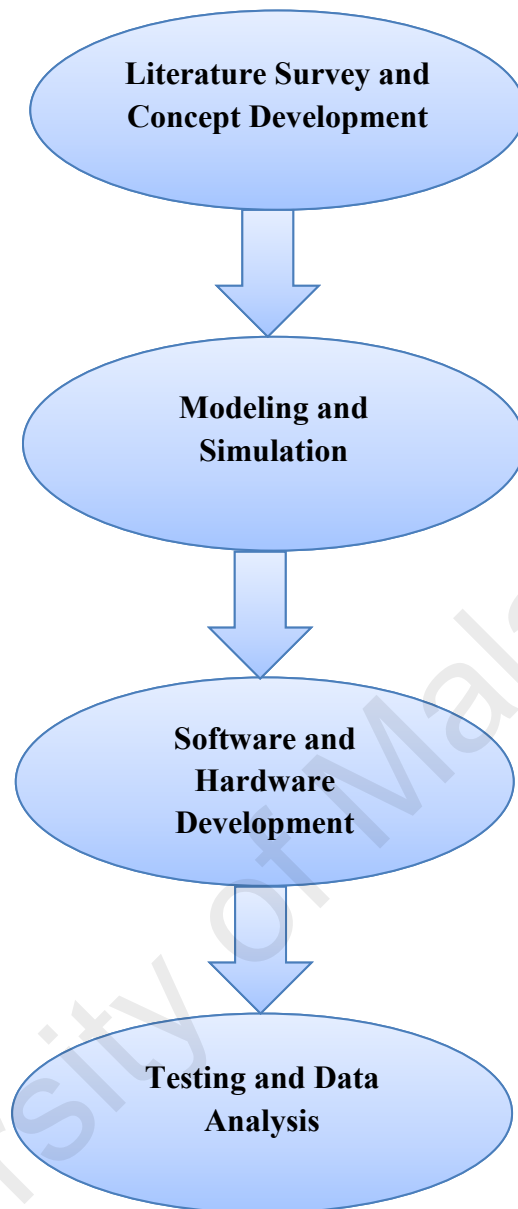


**Figure 1.4:** Flowchart of research methodology

### **1.5 Scope of Research**

This research study will focus only on the PI and PR current control technique of single-phase inverters. Both control techniques will be simulated and implemented in single-phase stand-alone inverter prototype and tested using resistive load. In order to compare the characteristics and the performance of the PI and PR controller tests are conducted at several operating conditions.

However, this study does not cover voltage control as it requires an additional control loop to be implemented for maintaining a sinusoidal output voltage. The controller's performances are verified based on experimental tests conducted on a 250 W single-phase inverter prototype.

## **1.6 Thesis Outline**

This thesis report is organized into five chapters. A brief summary of these five chapters is given in this section.

Chapter 2 gives an overview of current control techniques for single-phase inverters. In this chapter, the general structures of both linear and non-linear control techniques are presented including their transfer functions. The advantages and disadvantages of each controller are also given. Chapter 2 also covers the techniques used to mitigate the current harmonics, especially the low-order harmonics.

Chapter 3 presents the detail analysis and implementation of PI and PR current controllers. These include the mathematical modeling of the single-phase inverter, LC filter and the controllers. The controllers are analyzed in open-loop and closed-loop forms using bode plots. The explanations on hardware implementation for experimental verification are provided in this chapter.

Chapter 4 presents the results from the performance investigation of PI and PR control techniques for single-phase inverter. A brief comparison between PI and PR controllers in terms of harmonics suppression, steady-state response and transient response is also included in this chapter.

Chapter 5 presents the conclusion and future works.

## CHAPTER 2: AN OVERVIEW OF CURRENT CONTROL TECHNIQUES

### 2.1 Introduction

In this section, several important background concepts are introduced, and a brief review of the state-of-the-arts in current control techniques for single-phase inverters is presented. In a single-phase inverter, the challenge is to design a controller that can track a sinusoidal reference current. Several current control methods have been investigated in the literature for controlling such inverters (Teodorescu et al., 2004; Timbus et al., 2009; Zammit 2014). These current control methods can be classified into linear and nonlinear. Proportional integral (PI), proportional resonant (PR) and repetitive control (RC) are among the linear controllers while dead-beat (DB), hysteresis and predictive controls are the nonlinear types.

#### 2.1.1 Current Control Structures for Single-Phase Inverter

Figure 2.1 illustrates an example of the current control scheme implemented in a single-phase inverter with advanced power control in the case of grid-connected renewable energy system (Monfared & Golestan 2012). The actual grid current is measured and compared with the reference current where the error is fed to a current controller to produce the inverter PWM signals. For grid connected system voltage loop is not required since the grid voltage is regulated, unlike the standalone system which require additional control loop to maintain its output voltage.



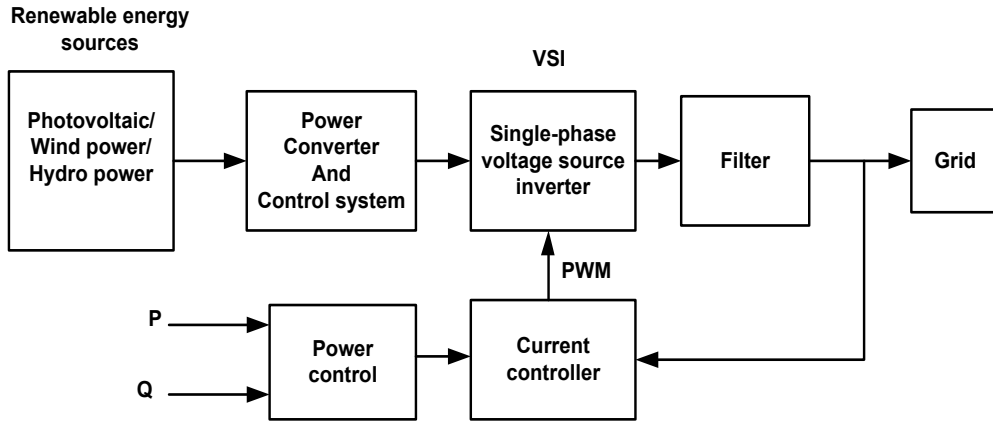


**Figure 2.1:** Structure of renewable power generation system with different energy sources

## 2.1.2 Linear Current Control for Single-Phase Inverters

### 2.1.2.1 Proportional-integral (PI) controller

PI controller is one of the most studied, well-known and established controllers in many applications, in which a constant or slowly-varying reference should be tracked (Espinoza et al., 2015; Y.-S. Kim et al., 2015; Pitalúa-Díaz et al., 2015; Wang et al., 2015). Most of the PI controllers are typically associated with  $dq$  control strategy since they are superior for controlling dc variables. The  $dq$  control is also called a synchronous reference frame control. A general structure of the  $dq$  control is shown in Figure 2.2 (Monfared & Golestan 2012).

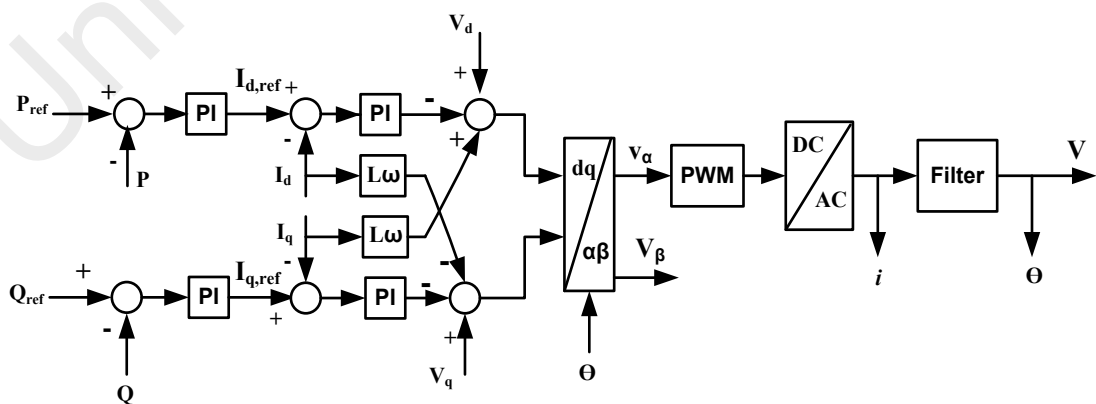


**Figure 2.2:** General current control structure for  $dq$ -control strategy

In this case, the dc-link voltage controller can be used to generate the reference current that represents the active power component. The reactive power reference is set depending on the need for the reactive power.

A conventional PI controller is defined by the following transfer function:

$$G_{PI}(s) = K_p + \frac{K_i}{s} \quad (2.1)$$

where,  $K_p$  and  $K_i$  are the proportional and integral gains of the controller. However, the low order harmonics compensation capability is very poor when using the PI controller in the system (Hassaine et al., 2014; Saccomando & Svensson, 2001; Teodorescu & Blaabjerg, 2004; Teodorescu et al., 2003; Twining & Holmes, 2002).

### 2.1.2.2 Proportional-resonant (PR) controller

Over the last decade, PR controller's popularity in current regulation for the stand-alone and grid-connected system has increased (Fukuda & Yoda, 2001; Hassaine et al., 2014; Teodorescu et al., 2006; Yuan 2002; Zmood & Holmes, 2003). Unlike PI controller, PR controller is able to track a sinusoidal current reference with zero steady-state magnitude and phase error in the stationary reference frame ( $\alpha\beta$  frame). The current control structure of PR controller in  $\alpha\beta$  frame is shown in Figure 2.3 (Monfared & Golestan 2012).

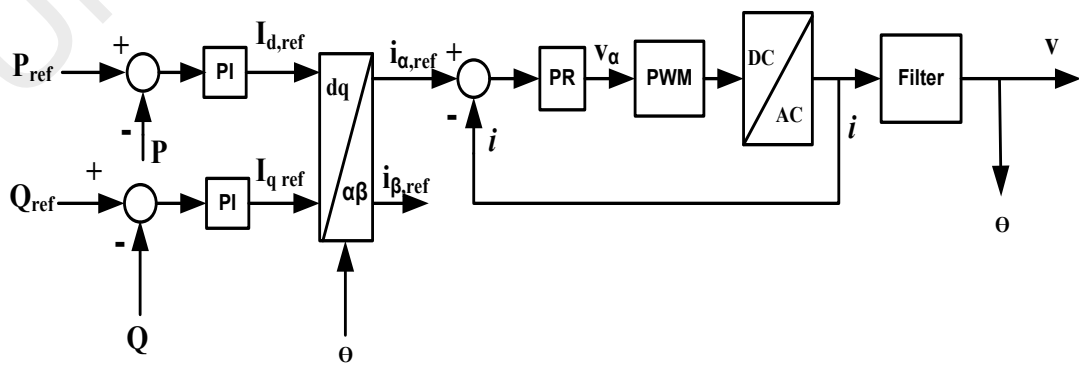
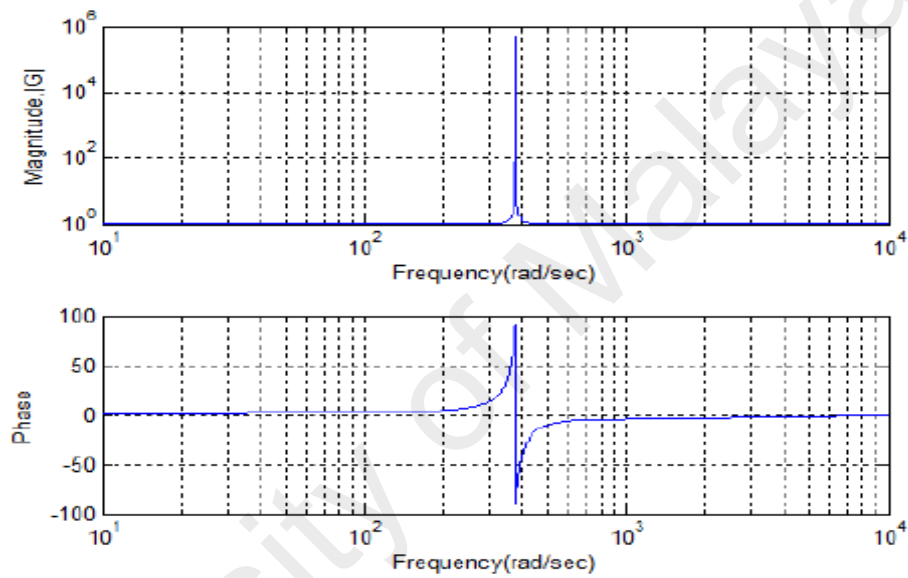


Figure 2.3: General current control structure for  $\alpha\beta$ -control strategy

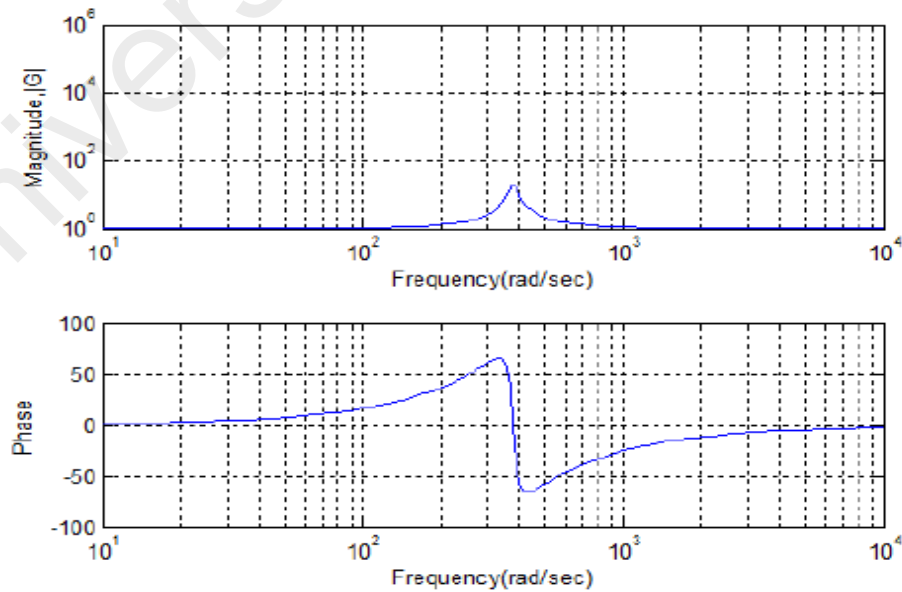
The transfer function of PR controller is defined as:

$$G_{PR}(s) = K_p + K_i \frac{s}{s^2 + \omega_0^2} \quad (2.2)$$

where,  $\omega_0$  is the resonance frequency,  $K_p$  is the proportional gain, and  $K_i$  is the integral gain of the controller. Equation (2.2) shows an ideal PR controller which can achieve an infinite gain and zero phase shift at the resonance frequency spectrum as shown in Figure 2.4 (a), depending on the value of the integral gain  $K_i$  (Teodorescu et al., 2006).



(a)



(b)

**Figure 2.4:** Frequency response (a) ideal PR controller; and (b) non-ideal PR controller; using  $K_p=1$ ,  $K_i=20$ ,  $\omega_0=314$  rad/s and  $\omega_c=10$  rad/s

To avoid the stability problem associated with an infinite gain, Equation (2.3) represents a non-ideal PR controller which is defined by:

$$G_{PR}(s) = K_p + K_i \frac{2\omega_c s}{s^2 + 2\omega_c s + \omega_0^2} \quad (2.3)$$

where  $\omega_c$  is the cut off frequency. The frequency response of Equation (2.3) is shown in Figure 2.4 (b), where the resonant peak has a finite gain of 50 dB which is satisfactorily high for eliminating the current tracking error.

### 2.1.2.3 Repetitive current (RC) controller

The repetitive current (RC) controller was constructed based on the internal model principle (IMP), where it is able to eliminate the steady-state error by periodically controlling its parameters (Z. Bin et al., 2008; Costa et al., 2004). The controller can achieve high gain at the integral multiples of fundamental frequency. The RC controllers are implemented as high order (e.g. 11<sup>th</sup> and 13<sup>th</sup>) harmonic compensator and the current controller is able to track the fundamental reference current (Keliang et al., 2009; Keliang et al., 2006). However, it was rather problematic, exhibiting a slow dynamic response that affects its stability (Costa et al., 2004). The block diagram of RC controller is shown in Figure 2.5. In order to obtain an optimal trade-off between practical realization and control performance, RC controllers are combined with PR controller (Yongheng et al., 2013).

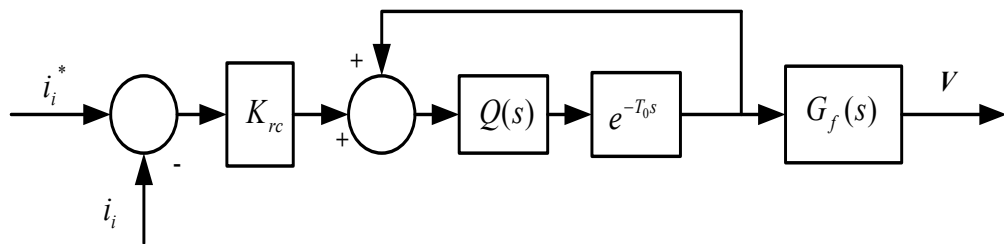


**Figure 2.5:** Block diagram of RC current controller

The transfer function of RC controller can be expressed as (Yongheng et al., 2013):

$$G_{RC}(s) = \frac{K_{rc} e^{-T_0 s} Q(s)}{1 - e^{-T_0 s} Q(s)} G_f(s) \quad (2.4)$$

where,  $K_{rc}$ , is the controller constants,  $Q(s)$  is the low-pass filter for increasing the stability of RC control system,  $T_0$  is the initial time period for grid voltage, and  $G_f(s) = e^{Ts}$  is a phase-lead compensation and  $T$  is the time period of phase-lead compensation. The repetitive controller can be expressed in discrete-time domain as (Yongheng et al., 2013):

$$G_{RC}(z) = \frac{K_{rc} z^{-N} Q(z)}{1 - z^{-N} Q(z)} Q_f(z) \quad (2.5)$$

where,  $N$  is the frequency ratio ( $N = \frac{f_s}{f_g}$ ),  $f_s$  and  $f_g$  are the sampling and the grid frequency, respectively.

### 2.1.3 Nonlinear Current Control for Single-Phase Inverters

#### 2.1.3.1 Dead-beat (DB) controller

The dead-beat controller which belongs to the family of predictive regulators is a popular control technique in many recent applications (Mattavelli et al., 2005; Mattavelli et al., 2003). When a dead-beat controller is well-tuned, it permits faster transient response among all digital current controllers. The discrete transfer function of the dead-beat controller is defined by (Blaabjerg et al., 2006):

$$G_{DB} = \frac{1 - az^{-1}}{b(1 - z^{-1})} \quad (2.6)$$

where  $a$  and  $b$  are represented by (2.7) and (2.8) respectively,

$$a = e^{-\frac{R_T T_s}{L_T}} \quad (2.7)$$

$$b = -\frac{1}{R_T} \left( e^{-\frac{R_T T_s}{L_T}} - 1 \right) \quad (2.8)$$

and  $R_T$  and  $L_T$  are the equivalent interfacing resistance and inductance of the inverter. The dead-beat controller has one sample time delay since it regulates the current such that it achieves its reference at the end of the next switching period. In this case, an observer must be implemented in the control structure to compensate for the time delay (Mattavelli et al., 2003), as shown in Figure 2.6 (Blaabjerg et al., 2006). Since the discrete transfer function of the observer is defined by,

$$F_{DB} = \frac{1}{1-z^{-1}} \quad (2.9)$$

Hence, the new current reference becomes,

$$i^{*'} = F_{DB}(i^* - i). \quad (2.10)$$

As a result, a fast and simple controller suitable for microprocessor-based application is obtained (Ito & Kawauchi, 1995).

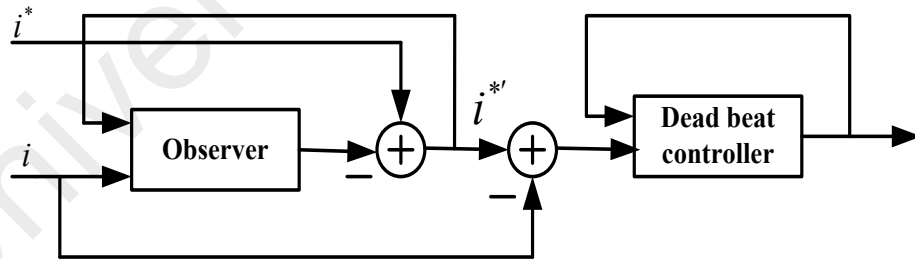


**Figure 2.6:** Block diagram of dead-beat controller

### 2.1.3.2 Hysteresis controller

Hysteresis control is a technique which can be used to control a current-controlled voltage source inverter where the reference current and the actual current are compared on an instantaneous basis to produce switching pulses for the inverter (Buso et al., 1999; Buso et al., 1998; Kazmierkowski & Malesani, 1998; Shukla et al., 2008). This method

controls switches in an inverter asynchronously to ramp the current up and down through an inductor so that it tracks the reference current signal. A configuration of hysteresis current controller is presented in Figure 2.7 (Hojabri et al., 2012). The error signal,  $e$  is the difference between the referent current and the actual current. Lower and upper limits associated with the minimum and maximum values of error signal are  $e_{min}$  and  $e_{max}$  respectively. The range of error signal ( $e_{min} - e_{max}$ ) where the output current of the inverter is controlled is called the hysteresis band. This allows the current to be kept within the upper and the lower hysteresis band limits as shown in Figure 2.8.

The advantages of the hysteresis control are simplicity, unconditioned-stability, independent of load parameters, robustness, and good transient response (Buso et al., 1999; Buso et al., 1998; Kazmierkowski & Malesani, 1998; Shukla et al., 2008).

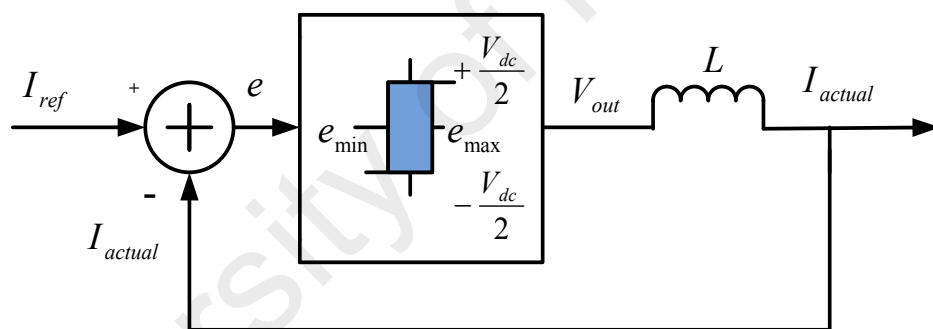


**Figure 2.7:** Configuration of hysteresis current controller

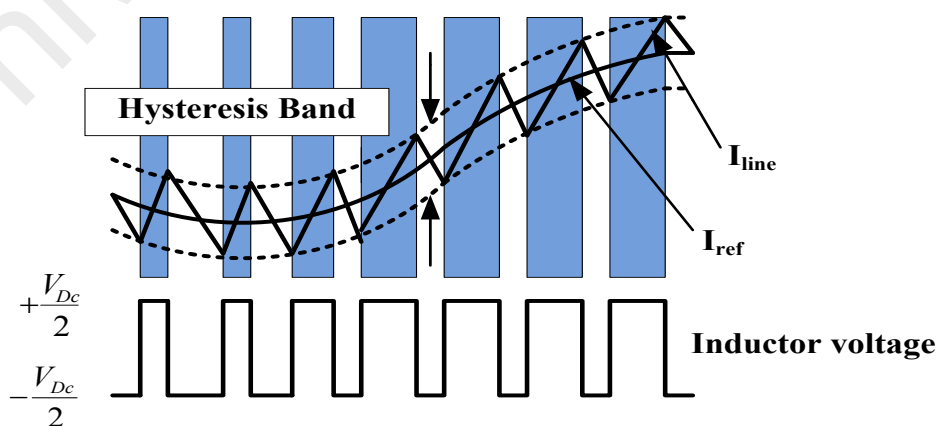


**Figure 2.8:** Hysteresis current controller operational waveform

### 2.1.3.3 Predictive controller

Predictive controller is well known for their ability to handle a system with nonlinearities. The predictive current control compromises the potential for achieving precise current control with low harmonic distortion and noise, but it is normally more difficult to be implemented (Y. Bin & Liuchen, 2005; Bode et al., 2005; Cortes et al., 2008; Gálvez-Carrillo et al., 2009; Mattavelli et al., 2005). The predictive controller calculates the inverter voltage required to force the output current to follow the current reference. A predictive current control scheme is shown in Figure 2.9 (Cortes et al., 2008; Hojabri et al., 2012) where the switching states  $S(k)$  and the output current  $i(k)$  are used to predict the characteristic of the system variables for each switching state.

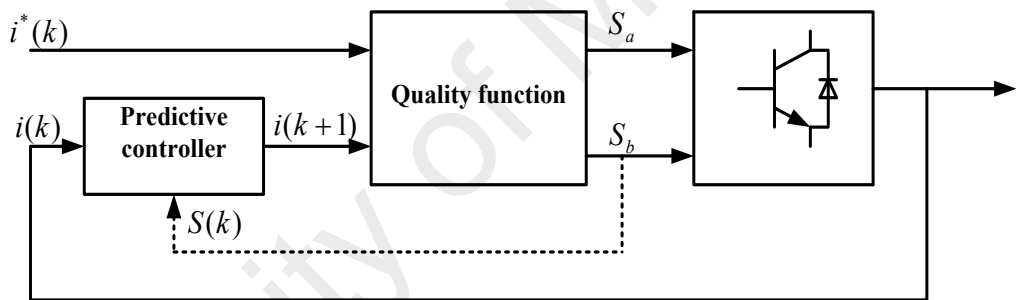


**Figure 2.9:** Block diagram of predictive controller

### 2.1.4 Analysis of Current Control Structures

Current regulation using PI controller in synchronous reference can achieve the same performance as the PR controller implemented in stationary reference frame. However, the control structure becomes more complicated which require voltage feed-forward and the cross-coupling terms. This makes PR controller more favorable for current regulation in single phase application since it is simpler. PLL is not a must for PR controller in grid-connected application, only the filtered voltage is needed to generate the current reference. For standalone application, look-up table can be used for the same purpose. In the case of non-linear controllers such as hysteresis, dead-beat and predictive controllers, the difficulty in terms of the current control operation becomes



higher when implemented in the stationary reference frame. Although the phase angle is not a must, these controllers generally require high sampling rate in order to achieve a superior performance. Observer is required for the dead-beat controller to compensate for the time delay, whereas, the predictive controller requires information on the system parameters for implementation.

### **2.1.5 Current Harmonics Compensation**

Nowadays, the use of electrical appliances driven by power electronics is increasing to produce and supply current at utility level. Hence, attention should be given so that the generation of current at unwanted frequencies may not grow without limit, because it may affect the public mains adversely. Therefore, the harmonics content on the public networks has to be restricted to a safe tolerance.

Similarly, for standalone inverter system where the inverter itself is the power source should be able to deliver high quality power to the load. In this case, the output voltage must contain a very low total harmonic distortion so that it produces very clean sinewave output. For current-controlled standalone inverter system, the output current should have relatively low current harmonics. Presently, there is no specific international standard for standalone system pertaining to voltage and current harmonics requirements. Only, those standards related to inverter system that is connected to the grid are available. Most international standards are addressing the harmonic limits of the electrical load or equipment that is supplied from the grid such as IEC 61000-3-2 and IEEE 519. In this section, several methods on how current harmonics can be compensated using different type of controllers are presented.

#### **2.1.5.1 Harmonics compensation using PI controllers**

For the implementation of PI controllers in  $dq$  control, the harmonic compensation can be applied based on low-pass and high-pass filters (Blaabjerg et al., 2006; de la

Parra et al., 2015; Newman et al., 2002). Therefore, the compensator can be designed such that specific current harmonics are eliminated. Due to load interruptions, the harmonic compensators are necessary for both positive and negative sequences of each harmonic order, thus increasing the complexity of control. For example, four compensators are required for the fifth and seventh harmonics compensation.

### 2.1.5.2 Harmonics compensation using PR controllers

The harmonics can be reduced further by incorporating the PR controller with selective harmonic compensation, especially for low-order harmonics. Usually, a harmonic compensator (HC) is designed to compensate for the 3<sup>rd</sup>, 5<sup>th</sup> and 7<sup>th</sup> harmonics (Blaabjerg et al., 2006; Teodorescu et al., 2004). However, an attempt to compensate high-order (e.g. the 11<sup>th</sup> and 13<sup>th</sup>) harmonics may introduce higher computational burden. The specific resonant gain ( $K_{ih}$ ) must be tuned to a comparatively high value for reducing the steady-state error. The main advantage is that only one harmonic compensator is needed to eliminate a harmonic order since it is able to work on both positive and negative sequences. A block diagram showing the resonant filter for filtering 3<sup>rd</sup>, 5<sup>th</sup>, 7<sup>th</sup> harmonics is shown in Figure 2.10.

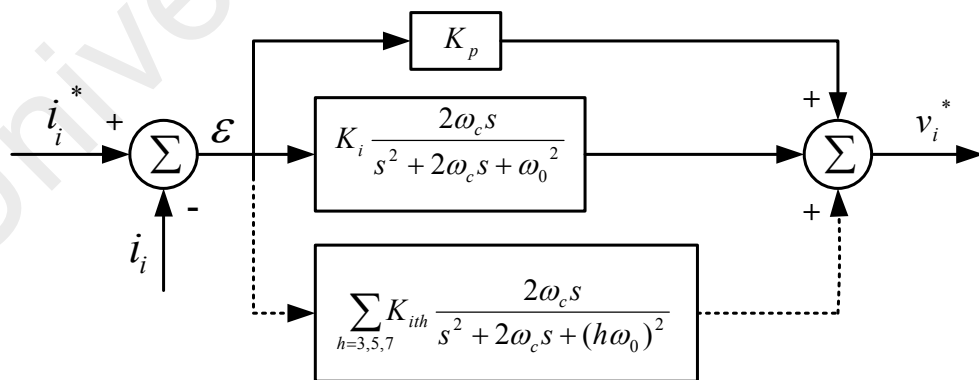


**Figure 2.10:** Block representation of harmonic compensator with PR controller

Based on PR controller, a series set of resonant blocks are utilized in particular to eliminate several selected low order odd harmonics (Blaabjerg et al., 2006; Teodorescu

et al., 2004; Teodorescu et al., 2006). Similar to PR controller, a series of resonant controllers cascaded together are tuned to the desired low order odd frequencies to further reduce current harmonics. The transfer function of non-ideal harmonic compensator (HC) and (PR+HC) to compensate the 3<sup>rd</sup>, 5<sup>th</sup> and 7<sup>th</sup> harmonics are given as (Teodorescu et al., 2006):

$$G_h(s) = \sum_{h=3,5,7} K_{ih} \frac{2\omega_c s}{s^2 + 2\omega_c s + (h\omega_0)^2} \quad (2.11)$$

$$G_{PR-h}(s) = K_p + \frac{2K_i \omega_c s}{s^2 + 2\omega_c s + \omega_0^2} + \sum_{h=3,5,7} K_{ih} \frac{2\omega_c s}{s^2 + 2\omega_c s + (h\omega_0)^2} \quad (2.12)$$

where,  $h$  is the harmonics number and  $K_{ih}$  is the specific resonant gain which must be tuned relatively high (but within stability limit) for the reducing the steady-state error (Lezana et al., 2007; Yuan 2002).

Since no transformations are necessary, this controller can be easily used in single-phase inverter systems. Figure 2.11 shows the bode diagram of harmonic compensation (HC) for 3<sup>rd</sup>, 5<sup>th</sup> and 7<sup>th</sup> harmonics with  $K_{ih}$  set to unity ( $K_{ih}=1$ ) and  $\omega_c = 1$  rad/s using Equation (2.11). Figure 2.12 shows the bode diagram of harmonic compensation for the summation of 3<sup>rd</sup>, 5<sup>th</sup> and 7<sup>th</sup> harmonics with  $\omega_c = 1$  rad/s and  $\omega_c = 10$  rad/s. whereas the bode diagram of PR+HC as shown in Figure 2.13 where,  $\omega_c = 1$  rad/s and  $\omega_c = 10$  rad/s based on Equation (2.12).

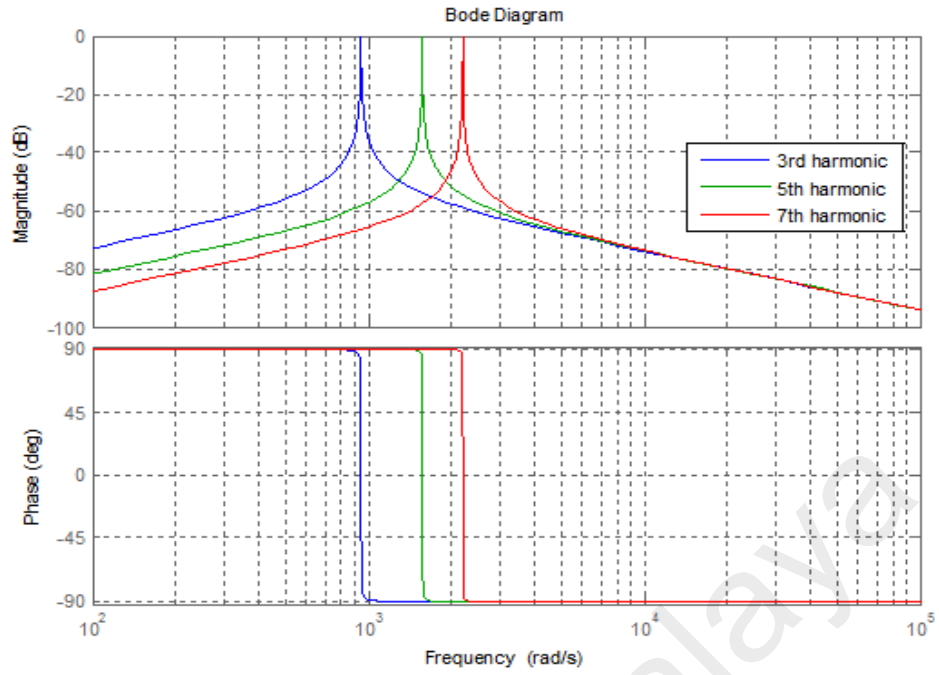


**Figure 2.11:** Bode diagram of HC for the individual of 3<sup>rd</sup>, 5<sup>th</sup> and 7<sup>th</sup> harmonic with  $K_{ih}=1$ ,  $\omega_c=1$  rad/s and  $\omega_o=314$  rad/s

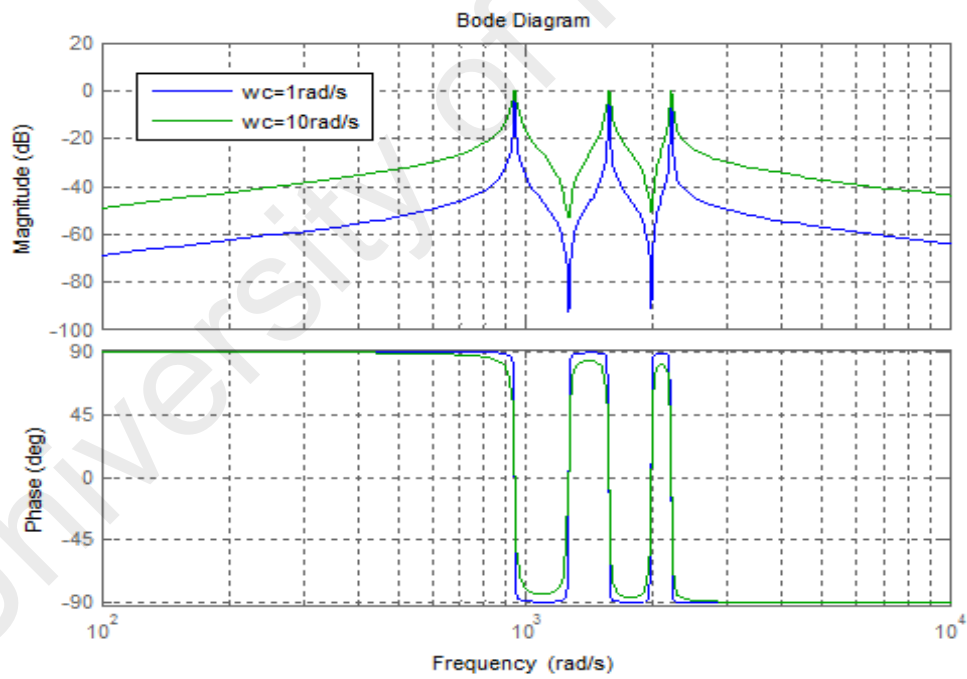


**Figure 2.12:** Bode diagram of HC for the summation of 3<sup>rd</sup>, 5<sup>th</sup> and 7<sup>th</sup> harmonics with  $K_{ih}=1$ ,  $\omega_c=1$  rad/s,  $\omega_c=10$  rad/s and  $\omega_o=314$  rad/s

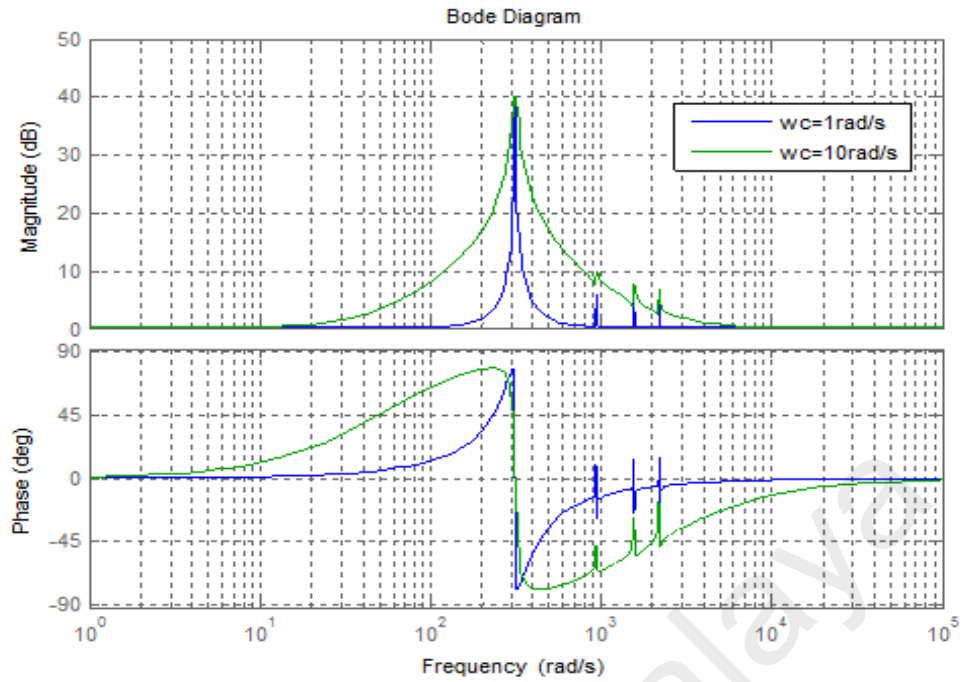


**Figure 2.13:** Bode diagram of PR+HC using  $K_p = 1$ ,  $K_i = 100$ ,  $K_{ih} = 1$ ,  $\omega_c = 1$  rad/s,  $\omega_c = 10$  rad/s and  $\omega_o = 314$  rad/s

### 2.1.5.3 Harmonics compensation using nonlinear controllers

Since nonlinear controllers such as dead-beat, predictive and hysteresis controllers have a very fast dynamic response, there is no issue for low-order harmonic compensation. The output current typically contains harmonics at the switching and sampling frequencies order. The only issue is that it requires fast sampling that could be a limitation in hardware implementation.

## 2.2 Summary

In this chapter, the comprehensive literature reviews of linear and non-linear current control techniques in terms of control structures, as well as harmonic compensation for single phase inverter application, have been performed.

## CHAPTER 3: ANALYSIS AND IMPLEMENTATION OF PI AND PR CURRENT CONTROLLERS

### 3.1 Introduction

The design and development of LC-filter, PR current controller, frequency response for open loop and closed-loop controller and experimental setup have been described in this chapter. In this chapter, both controllers of PI and PR are implemented in hardware setup using difference equation have been presented.

### 3.2 Single-Phase PWM Inverter

PWM inverters are extensively used in various applications such as ac drives, energy conversion, power conditioning devices and many more. The schematic diagram of a single-phase inverter is shown in Figure 3.1. In this study, unipolar PWM method is used instead of bipolar PWM to achieve a better inverter output quality at the same switching frequency. Since the inverter produces high switching frequency components, it has to be filtered out to generate a clean sinusoidal output.

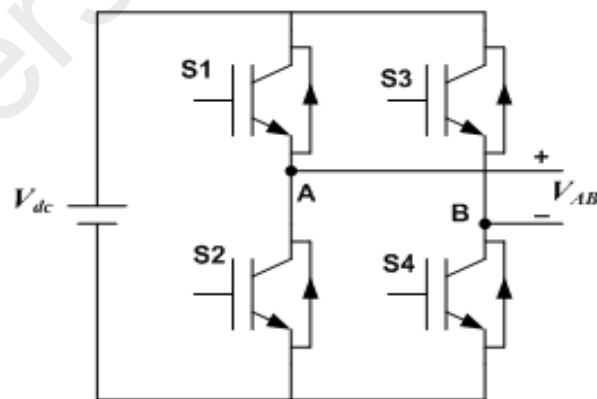


**Figure 3.1:** Schematic diagram of a single-phase inverter

A power filter is therefore required and can be classified into active and passive filters. Passive filter is chosen in this study since it is simple and easier to be implemented. There is a first order passive L-filter, which consists only inductor

component that can attenuate current ripples due to inverter switching (Hobraiche et al., 2009; Kim & Sul January 2011; H. Kim et al., 2008). The limitation of L-filter is the size which is very bulky especially when the system deals with high power. The second order LC-filter is used to control both the output current and voltage which is the reason why it is very useful for standalone application (Hobraiche et al., 2009; H. Kim & Sul, 2005; Kim & Sul January 2011). The alternative third order LCL-filter offer smaller filter size at lower switching frequencies as compared to the other two filters for the same level of current harmonics. However, due to resonance it can cause steady-state and transient problems for the output current (Gabe et al., 2009; Liserre et al., 2005; Park et al., 2008). In this study, as a tradeoff LC-filter is chosen for hardware implementation. Figure 3.2 shows an inverter supplying power to the load through the LC-filter.

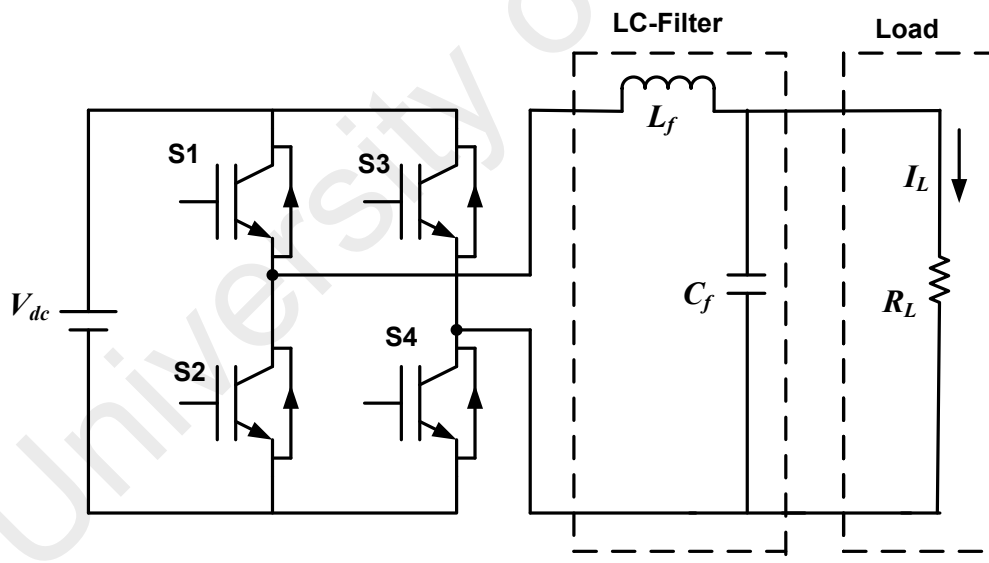


**Figure 3.2:** Inverter supplying power to load through the LC-filter

### 3.3 Current Control Scheme for Single-Phase Inverter with LC-Filter

This section describes a control method for single-phase inverter system which can provide low harmonics content in the output current waveform. The PR controller reduces the computational burden and control efforts while attaining frequency response

characterized similarly to PI controller. Moreover, with PR controller selective harmonics compensation technique can be implemented without any excessive requirements particularly for non-linear load (Abdel-Qawee et al., 2013). Figure 3.3 illustrates a block diagram of a current control scheme for single-phase inverter with LC-filter.

In this figure, there is only one current control loop to regulate the inverter output current to be sinusoidal. First, the current error is obtained by comparing the reference current generated and the measured load current. Then, the error will be fed to the PR controller and the output is the modulating signal used for PWM switching signals generation. The output voltage is not controlled in which its magnitude depends on the amount of current flows into the load. For stand-alone applications, the control scheme usually consists of two cascaded loops. One is the internal current loop, which is used to regulate the load current, and another is the outer voltage loop, which is used to maintain the sinusoidal output voltage (Agirman & Blasko, 2003; Huibin et al., 2003; Teodorescu et al., 2004).

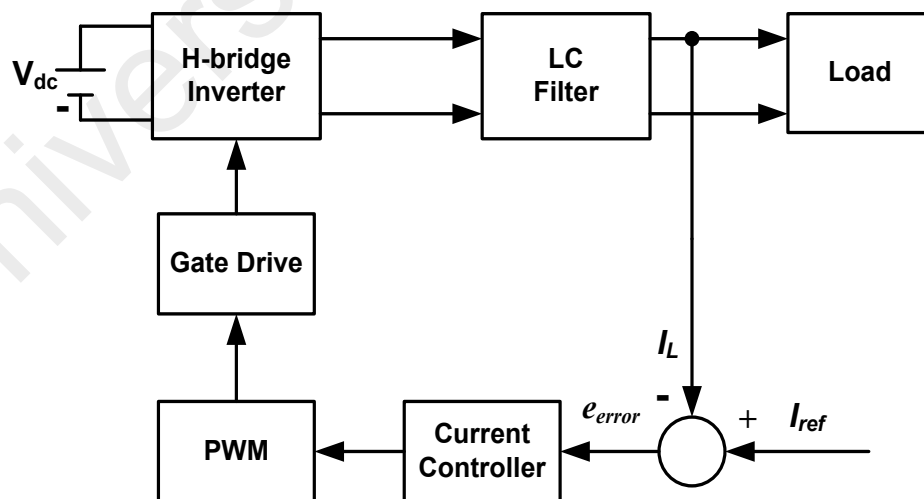


**Figure 3.3:** Block diagram of a current control scheme for single-phase inverter with LC-filter



### 3.3.1 Analysis the Design of Filter Parameters

A second order low pass LC filter can be used to obtain lower total harmonic distortion (THD) due to inverter switching and to improve the quality of the output power (Abdel-Qawee et al., 2013; Chen et al., 1992; Chiang et al., 1996). Figure 3.4 shows the equivalent circuit of an LC-filter.

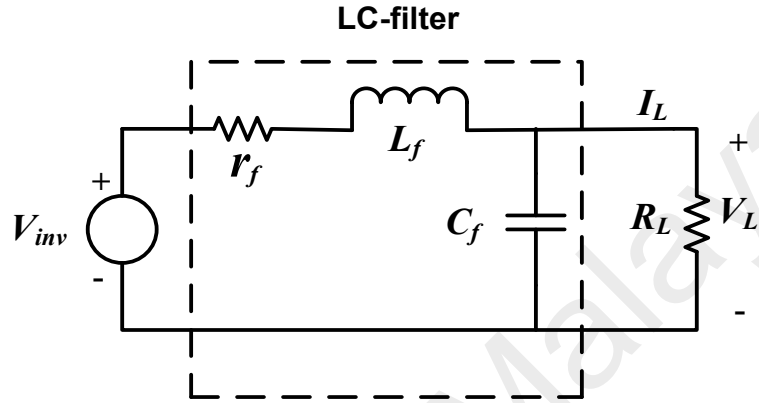


**Figure 3.4:** Equivalent circuit of an LC-filter

where,  $L_f$  is the filter inductor,  $r_f$  is the internal resistance of the filter inductor,  $C_f$  is the filter capacitor,  $R_L$  is the load resistor,  $V_{inv}$  is the inverter output voltage and  $V_L$  is the output load voltage.

The resonance frequency of the low pass LC filter is defined as below:

$$f_{res} = \frac{1}{2\pi\sqrt{L_f C_f}} \quad (3.1)$$

Assuming  $r_f$  is small and negligible, the transfer function of the LC filter is given by the following equation:

$$G_f(s) = \frac{\frac{1}{sC_f}}{\frac{1}{sC_f} + sL_f} \quad (3.2)$$

The frequency response of the LC filter is shown in Figure 3.5 in the case of  $L = 5$  mH and  $C = 0.22$   $\mu$ F are selected. From the figure, the resonance frequency of the filter is 4.79 kHz and the filter gives about -25 dB attenuation of the inverter current at 20 kHz switching frequency. Therefore, current ripple will be highly attenuated.

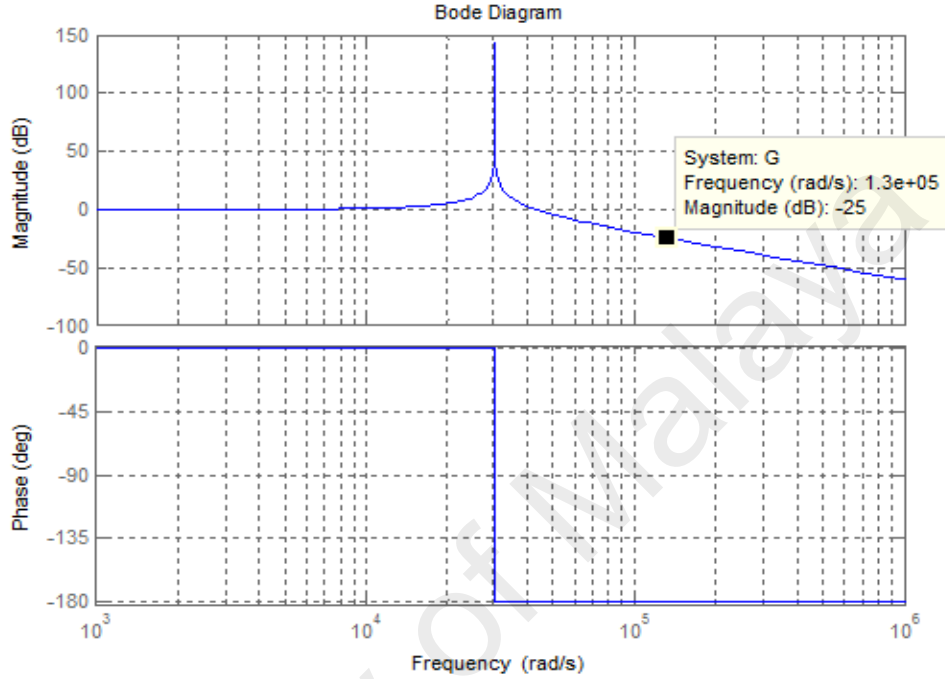


**Figure 3.5:** Frequency response of LC filter with  $L = 5$  mH and  $C = 0.22$   $\mu$ F

The overall transfer function of the inverter with LC filter and resistive load can be expressed by the following equation:

$$G_F(s) = \frac{V_L(s)}{V_{inv}(s)} = \frac{\frac{1}{sC_f} \parallel R_L}{\frac{1}{sC_f} \parallel R_L + sL_f} \quad (3.3)$$

$$G_F(s) = \frac{V_L(s)}{V_{inv}(s)} = \frac{1}{s^2 + \left(\frac{1}{R_L C_f}\right)s + \frac{1}{L_f C_f}} \quad (3.4)$$

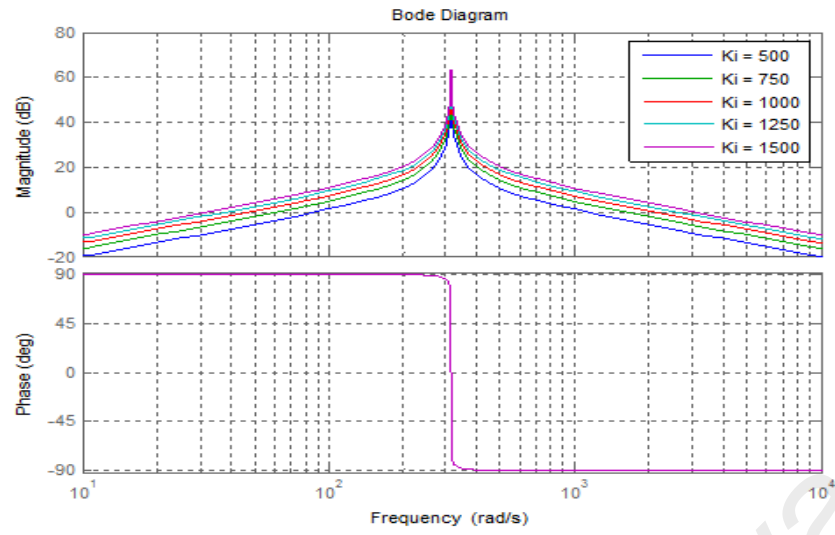
### 3.3.2 Analysis the Design of PR Current Controller

The design and analysis of PR controller is normally performed by using Bode diagrams and phase margin criterion, and to study the stability by means of the phase margin at the crossover frequency defined by the proportional gain (Bojoi et al., 2008; Castilla et al., 2009). In many applications, analysis using Bode diagrams is enough to achieve satisfying results. A more systematic method by means of Nyquist diagrams can also be used to tune the PR controller parameters which can give higher stability and improved performance (Basic et al., 2001; Bojoi et al., 2008).

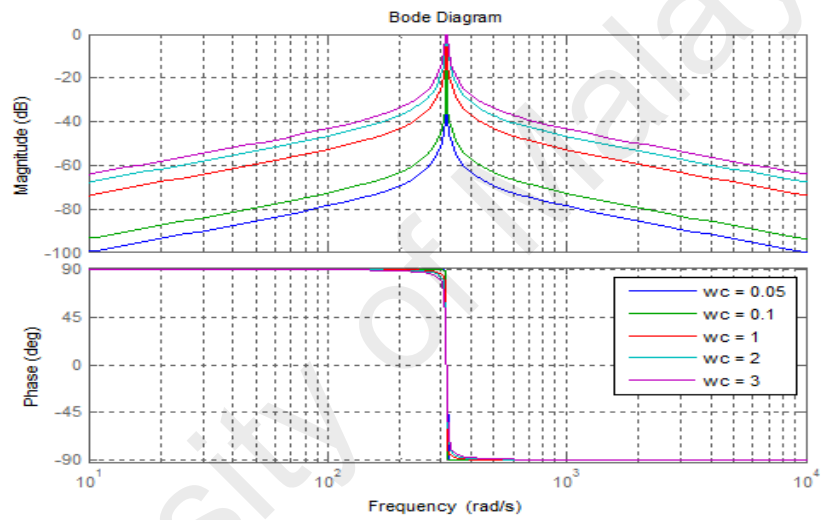
#### 3.3.2.1 Frequency response of open-loop non-ideal PR controller

The response of non-ideal PR controller has been described in chapter 2, as shown in Equation (2.3) is comparable to that of the ideal PR controller. From the equation, it is clear that there are three parameters in the non-ideal PR controller comprising  $K_p$ ,  $K_i$  and  $\omega_c$ . In order to investigate the effect of the controller parameters on the PR controller's performance, one of the parameters will be varied while the other parameters will be kept constant. Figure 3.6 (a) shows the open-loop frequency response of the controller in terms of the magnitude and phase when  $K_i$  is varied while  $K_p = 0$  and  $\omega_c = 1$  rad/s.

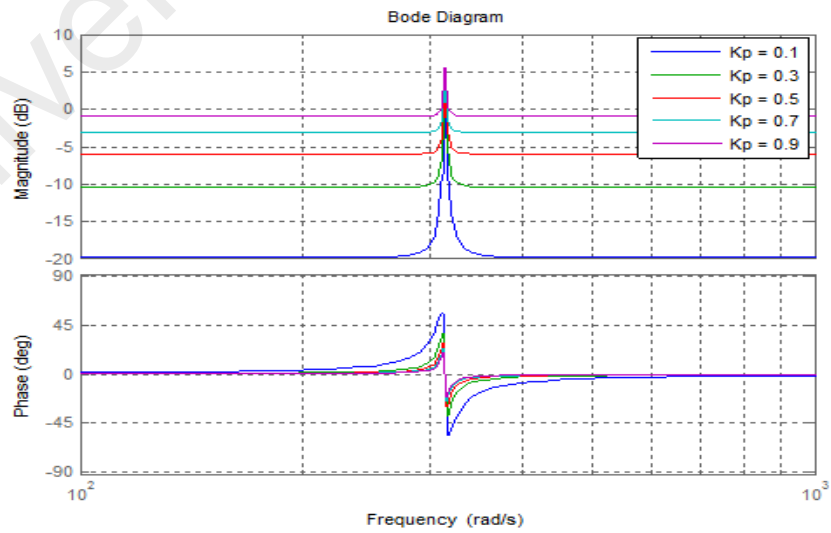
It can be observed that the magnitude of the PR controller gain increases when  $K_i$  is increased. But  $K_i$  has no effect on the bandwidth of the system as seen from the phase response of the PR controller. Assuming  $K_p = 0$ ,  $K_i = 1$ , the change of  $\omega_c$  has an effect on both the magnitude and the phase of the PR controller. Both the magnitude and the phase increase when  $\omega_c$  is increased, as shown in Figure 3.6 (b).



(a)



(b)



(c)

**Figure 3.6:** Frequency of the non-ideal PR controller as a function of (a)  $K_i$  changes, (b)  $\omega_c$  changes and (c)  $K_p$  changes

When  $K_i = 1$ ,  $\omega_c = 1$  rad/s and the proportional gain  $K_p$  is varied, the magnitude of PR controller increases, but the phase of PR controller decreases, as shown in Figure 3.6 (c). To obtain the best output response the controller need to be tuned appropriately. A tuning method given in (Guo et al., 2006; Zmood & Holmes, 2003) can be used for this purpose. Generally, a suitable  $\omega_c$  should be selected to provide a reasonable bandwidth around the resonance frequency.  $K_p$  is then selected to ensure that superior performance in sinusoidal reference tracking could be attained. Finally,  $K_i$  is selected so that the steady-state errors in both magnitude and phase are eliminated.

According to the analysis from the frequency response of open-loop non-ideal PR controller, the best values are selected,  $K_p = 0.5$ ,  $K_i = 1000$  and  $\omega_c = 0.1$  rad/s. Figure 3.7 shows the Bode plot of open-loop PR controller in MATLAB using the selected values. From Figure 3.7, the following points have been satisfied, (Alexandra et al., 2013; Hanju et al., 2009; Khairy et al., 2011; Lee 2012; Teodorescu et al., 2006; Teodorescu et al., 2011).

- i. Gain margin is finite and relatively high to achieve small steady-state error.
- ii. Stability is maintained as phase is always kept below  $180^\circ$ ,
- iii. Wide bandwidth reduces sensitivity to slight frequency variation.

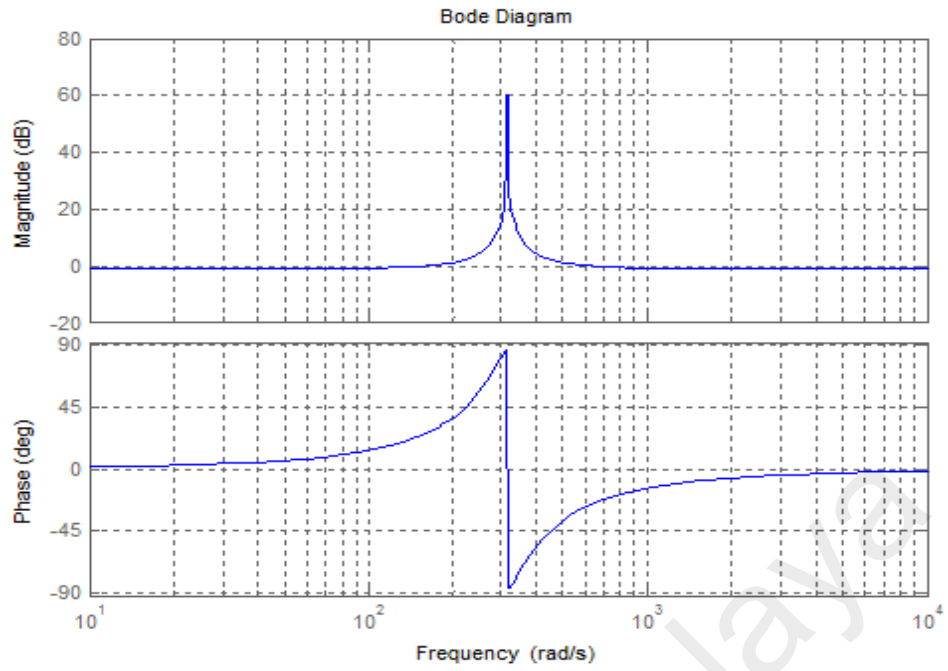


**Figure 3.7:** Bode plot of open-loop non-ideal PR controller ( $K_p = 0.5$ ,  $K_i = 1000$  and  $\omega_c = 0.1$  rad/s)

### 3.3.2.2 Frequency response of closed-loop control system

For comparison, both the closed-loop transfer functions of the PI and PR current controllers are analyzed. The block diagram of a closed-loop current control scheme used for the comparison is shown in Figure 3.8.

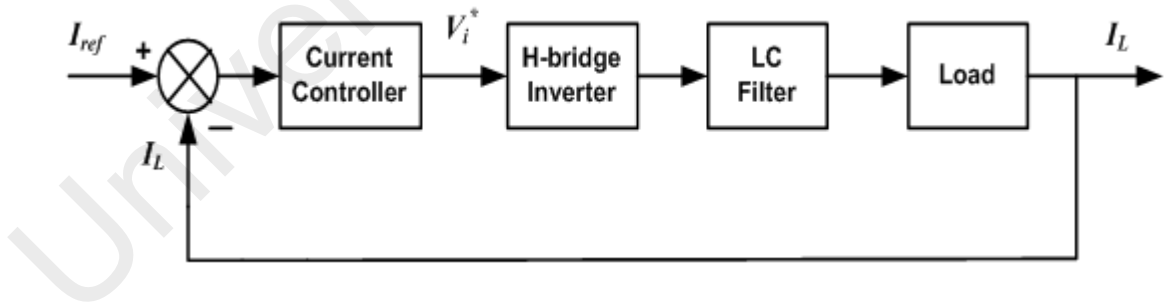


**Figure 3.8:** Block diagram of closed-loop current control scheme

The closed-loop transfer function of the system using PI controller can be defined as:

$$M_{PI}(s) = \frac{I_L}{I_{ref}} = \frac{G_{PI}(s)G_I(s)G_F(s)}{1 + G_{PI}(s)G_I(s)G_F(s)} \quad (3.5)$$

where,  $G_{PI}(s) = K_p + \frac{K_i}{s}$ ,  $G_I(s) = K$  and  $G_F = \frac{R_L}{R_L L_f C_f s^2 + L_f s + R_L}$  are the transfer functions of the PI controller, the inverter and the filter including the load respectively.

Substituting all the transfer functions yields the complete transfer function of the system which is represented by Equation (3.6).

$$M_{PI}(s) = \frac{K\{K_p s + K_i R_L\}}{R_L L_f C_f s^3 + L_f s^2 + (R_L + K K_p R_L)s + K K_i R_L} \quad (3.6)$$

Similarly, the closed-loop transfer function of the system using PR controller can be defined as below:

$$M_{PR}(s) = \frac{I_L}{I_{ref}} = \frac{G_{PR}(s)G_I(s)G_F(s)}{1 + G_{PR}(s)G_I(s)G_F(s)} \quad (3.7)$$

$$\text{where, } G_{PR}(s) = K_p + K_i \frac{2\omega_c s}{s^2 + 2\omega_c s + \omega_0^2}, G_I(s) = K \text{ and } G_f = \frac{R_L}{R_L L_f C_f s^2 + L_f s + R_L}$$

are the transfer functions of the PR controller, the inverter and the filter including the load respectively. The complete transfer function of the system can be obtained as Equation (3.8) below.

$$M_{PR}(s) = \frac{K\{K_p R_L s^2 + 2(K_p \omega_c R_L + K_i \omega_c R_L)s + K_p \omega_0^2 R_L\}}{\lambda_4 s^4 + \lambda_3 s^3 + \lambda_2 s^2 + \lambda_1 s + \lambda_0} \quad (3.8)$$

where,

$$\lambda_4 = L_f C_f; \lambda_3 = (L_f + 2\omega_c L_f C_f R_L);$$

$$\lambda_2 = (R_L + 2\omega_c L_f + L_f C_f R_L \omega_0^2 + K K_p R_L);$$

$$\lambda_1 = (2\omega_c R_L + \omega_0^2 L_f + 2K K_p \omega_c R_L + 2K K_i \omega_c R_L); \text{ and } \lambda_0 = (\omega_0^2 R_L + K K_p \omega_0^2 R_L)$$

Figure 3.9 and Figure 3.10 show the frequency responses of the closed-loop PI and PR current control systems respectively.

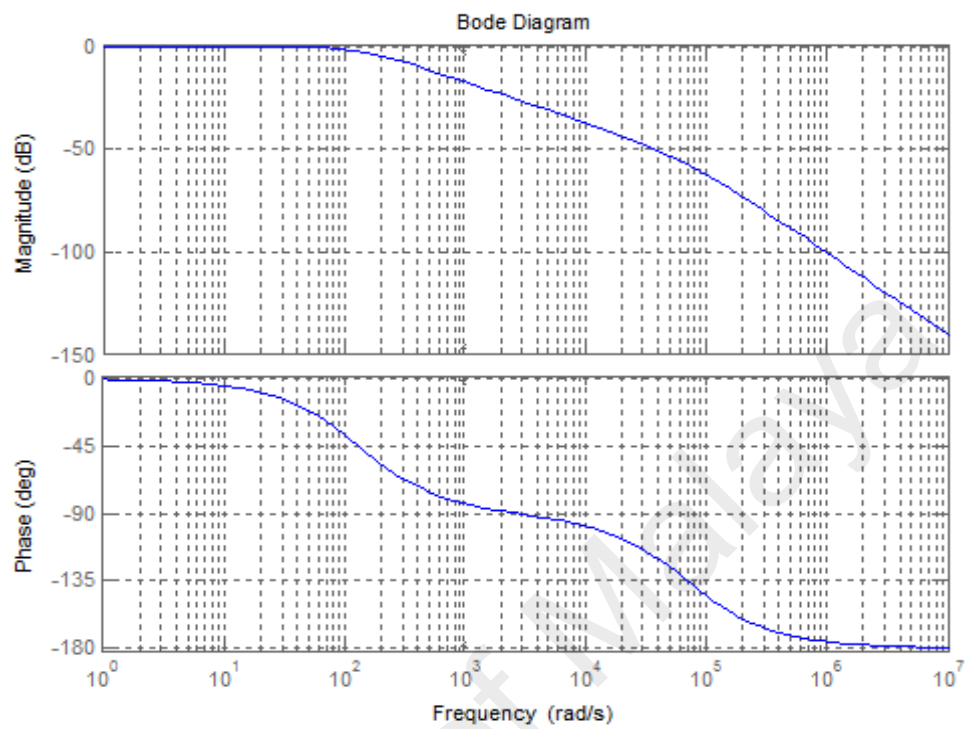


**Figure 3.9:** Frequency response of closed-loop transfer function using PI controller ( $K_p = 0.5$  and  $K_i=200$ )

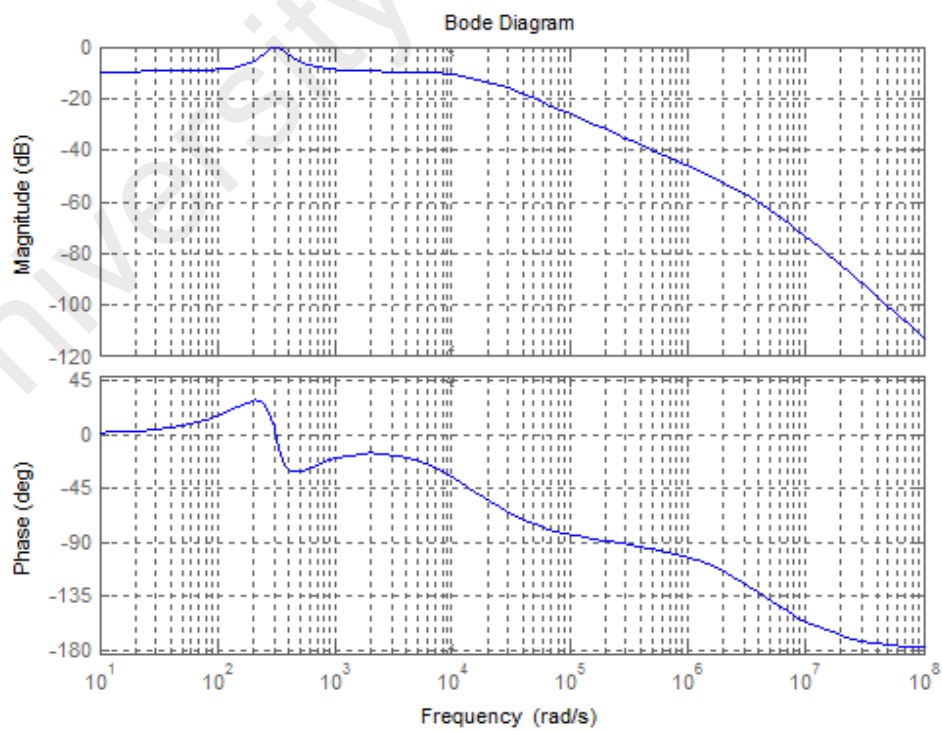


**Figure 3.10:** Frequency response of closed-loop transfer function using PR controller ( $K_p = 0.5$ ,  $K_i=1000$ ,  $\omega_0 = 314$  rad/s and  $\omega_c = 0.1$  rad/s)



### 3.4 Implementation of PI Controller Using Discrete Transfer Function

The discrete transfer function of the PI controller can be obtained by applying bi-linear transformation and substituting  $s = \frac{2(z-1)}{T(z+1)}$  into in Equation (2.1). This yields the following transfer function in z-domain;

$$G_{PI}(z) = \frac{b_0 + b_1 z^{-1}}{a_1 + a_2 z^{-1}} \quad (3.9)$$

where  $T$  is the sampling time and:

$$b_0 = K_p + K_i \frac{T}{2} \quad (3.10)$$

$$b_1 = -2K_p + K_i \frac{T}{2} \quad (3.11)$$

$$a_1 = 1 \quad (3.12)$$

$$a_2 = -1 \quad (3.13)$$

The discrete equation of the PI controller for hardware implementation is given as:

$$u(n) = \frac{b_0}{a_1} e(n) + \frac{b_1}{a_1} e(n-1) - \frac{a_2}{a_1} u(n-1) \quad (3.14)$$

Finally, the difference equation of PI controller becomes,

$$u(n) = b_0 e(n) + b_1 e(n-1) + u(n-1) \quad (3.15)$$

where,

$u(n)$  = present controller output,

$u(n-1)$  = previous controller output,

$e(n)$  = present error,

$e(n-1)$  = previous error.

Based on the optimized PI controller parameters ( $K_p = 0.5$  and  $K_i = 200$ ), the coefficient of PI controller becomes,  $b_0 = 0.505$ ,  $b_1 = -0.995$ ,  $a_1 = 1$  and  $a_2 = -1$ .

The transfer function in z-domain PI controller is given as:

$$G_{PI}(z) = \frac{0.505 - 0.995z^{-1}}{1 - z^{-1}} \quad (3.16)$$

### 3.5 Implementation of PR Controller Using Discrete Transfer Function

The non-ideal PR controller represented by Equation (2.3) makes the controller more easier to be implemented in the digital system due to their finite precision (Zammit 2014; Zmood & Holmes, 2003). The discrete transfer function of the non-ideal PR controller can be obtained by applying bi-linear transformation and putting  $s = \frac{2(z-1)}{T(z+1)}$

into in Equation (2.3). This yields the following transfer function in z-domain;

$$G_{PR}(z) = K_p + \frac{2K_i\omega_c \frac{2(z-1)}{T(z+1)}}{\frac{4(z-1)^2}{T^2(z+1)^2} + 2\omega_c \frac{2(z-1)}{T(z+1)} + \omega_0^2} \quad (3.17)$$

where  $T$  is the sampling time. Equation (3.16) can be rearranged in the following form in terms of the controller's output  $U(z)$  and the error  $E(z)$ .

$$G_{PR}(s) = \frac{U(z)}{E(z)} = \frac{b_0 + b_1z^{-1} + b_2z^{-2}}{1 + a_1z^{-1} + a_2z^{-2}} \quad (3.18)$$

where,

$$b_0 = \frac{(4 + 4T\omega_c + \omega_0^2 T^2)K_p + 4K_i T\omega_c}{4 + 4T\omega_c + \omega_0^2 T^2} \quad (3.19)$$

$$b_1 = \frac{(2\omega_0^2 T^2 - 8)K_p}{4 + 4T\omega_c + \omega_0^2 T^2} \quad (3.20)$$

$$b_2 = \frac{(4 - 4T\omega_c + \omega_0^2 T^2)K_p - 4K_i T\omega_c}{4 + 4T\omega_c + \omega_0^2 T^2} \quad (3.21)$$

$$a_1 = \frac{2\omega_0^2 T^2 - 8}{4 + 4T\omega_c + \omega_0^2 T^2} \quad (3.22)$$

$$a_2 = \frac{4 - 4T\omega_c + \omega_0^2 T^2}{4 + 4T\omega_c + \omega_0^2 T^2} \quad (3.23)$$

Finally, the difference equation of the PR controller for hardware implementation is given as:

$$u(n) = b_0 e(n) + b_1 e(n-1) + b_2 e(n-2) - a_1 u(n-1) - a_2 u(n-2) \quad (3.24)$$

where,

$u(n)$  = present controller output,

$u(n-1)$  = previous controller output,

$u(n-2)$  = earlier controller output,

$e(n)$  = present error,

$e(n-1)$  = previous error,

$e(n-2)$  = earlier error.

Based on the optimized the PR controller parameters ( $K_p = 0.5$ ,  $K_i = 1000$  and  $\omega_c = 0.1$  rad/s), the co-efficient of PR controller becomes,  $b_0 = 0.504999$ ,  $b_1 = -0.99987$ ,  $b_2 = 0.494995$ ,  $a_1 = -1.9997$  and  $a_2 = 1$ .

The transfer function in z-domain PR controller is given as:

$$G_{PR}(s) = \frac{U(z)}{E(z)} = \frac{0.504999 - 0.99987z^{-1} + 0.494995z^{-2}}{1 - 1.9997z^{-1} + z^{-2}} \quad (3.25)$$

### 3.6 Experimental Design and Setup

Figure 3.11 shows the block diagram of the experimental design showing the connections between the inverter, digital signal processor (DSP) board, sensors, gate drive circuit and the phase-locked-loop (PLL) source.

The hardware prototype that has been developed for testing the performance of both PI and PR current controllers is shown in Figure 3.12. The inverter is connected to the resistive load through the LC filter. For implementation of both controllers' algorithms, a 32-bit floating-point TMS320F28335 eZdsp development board was used. The C program for both controllers was developed by using Texas Instrument Code Composer Studio 6.0 (CCS) software. The inverter switching frequency was set to 20 kHz and the dead band was set to 1.3  $\mu$ s, since the load is less inductive. The PWM pulses were generated through the internal PWM module of the DSP. Voltage and current signals were measured by using the 12-bit analog-to digital converter (ADC) built inside the eZdsp development board. Sinusoidal reference signal was generated by sensing the grid voltage and using the phase-locked-loop module. The power electronic switches used were IGBT module. The major parameters of the prototype are listed in Table 3.1.

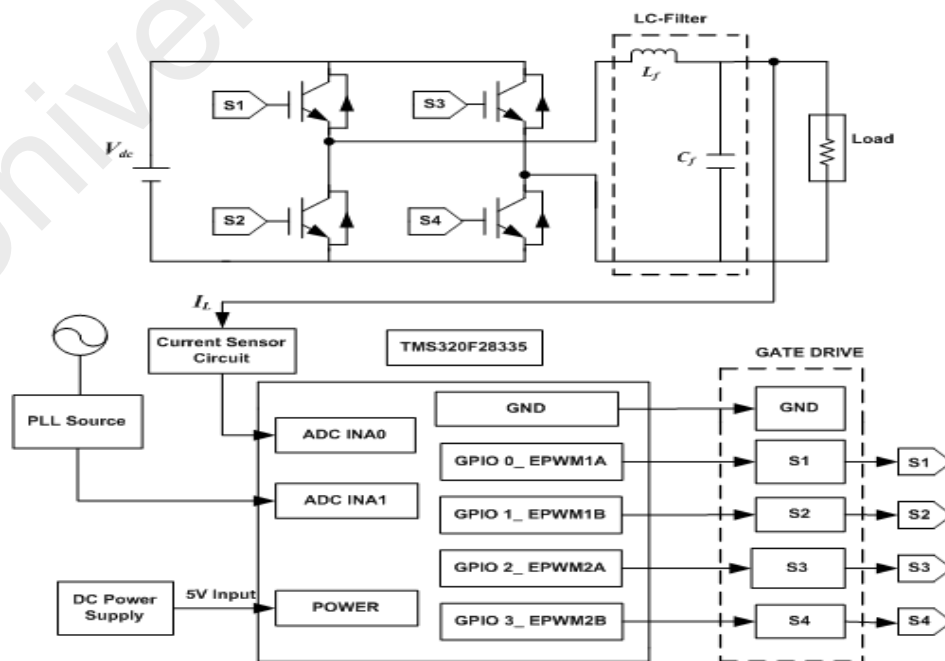
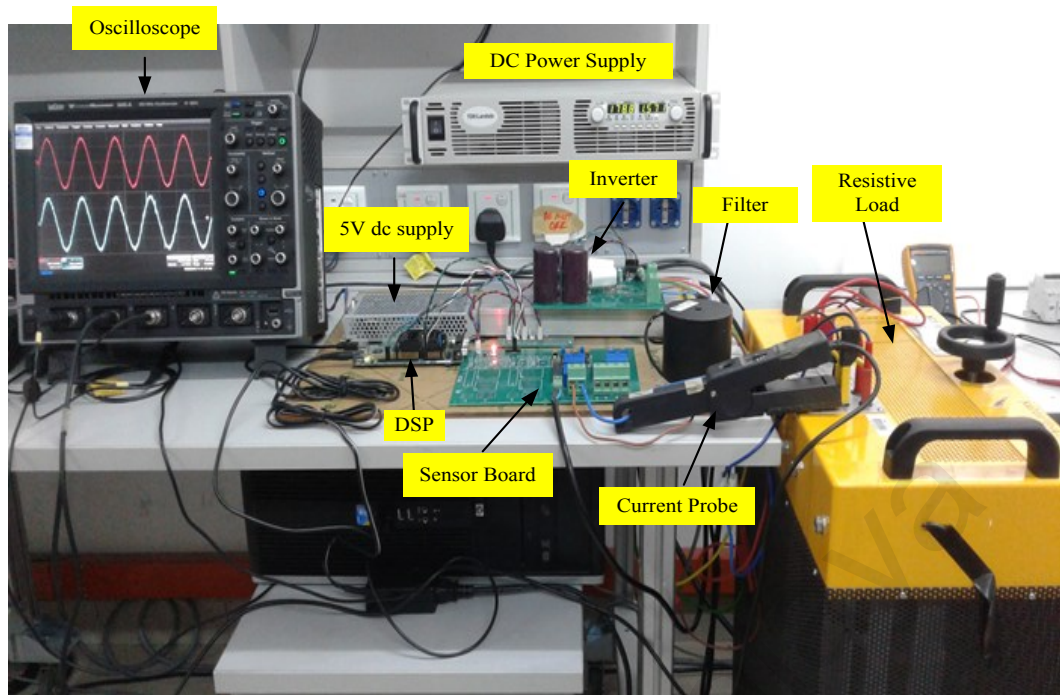
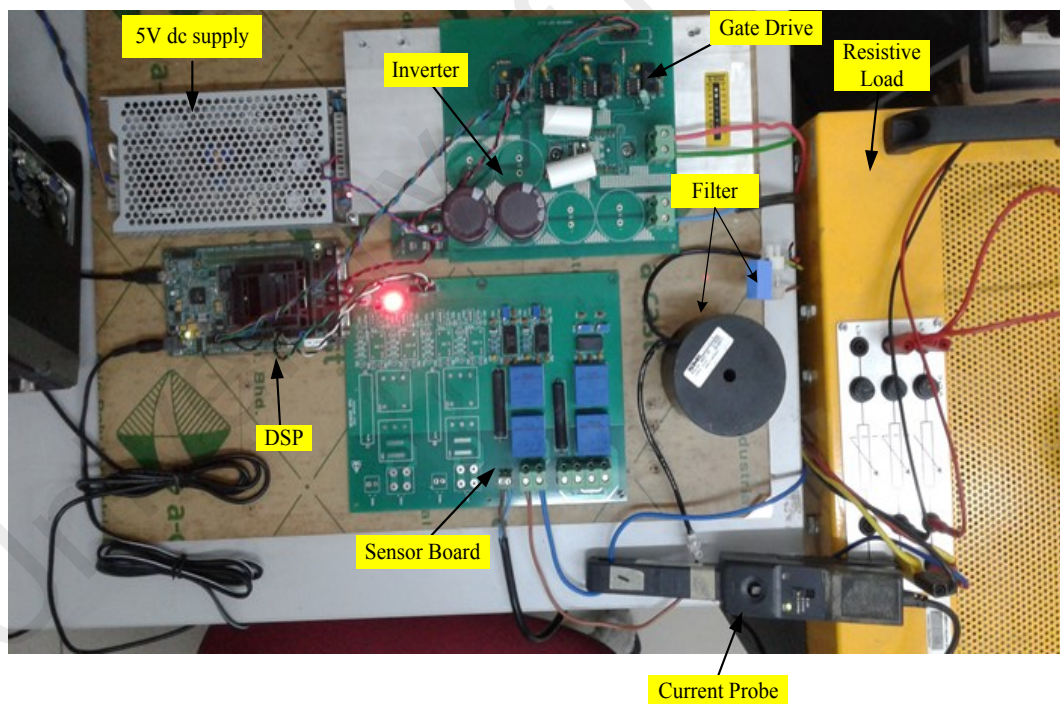


Figure 3.11: Block diagram of experimental design



(a) Front view



(b) Top view

**Figure 3.12:** Prototype setup of the single-phase inverter using resistive load (a) Front view and (b) Top view

**Table 3.1:** Inverter specifications.

<b>Parameters</b>	<b>Value</b>
DC voltage, $V_{dc}$	180 V
IGBT Module (S1-S4)	INFINEON (F4-50R06W1E30)
Voltage transducer	LEM LV25 - P
Current transducer	LEM LA25 – NP
Filter inductor, $L_f$	5 mH
Filter capacitance, $C_f$	0.22 $\mu$ F
Resistor, $R_L$	50 $\Omega$
Switching frequency, $f_s$	20 kHz

### 3.7 Summary

The design details of PI and PR controllers including LC filter are presented in this chapter. This includes open loop & closed loop frequency response analysis for both controllers. In the last section, details on hardware implementation and testing are presented.

## CHAPTER 4: RESULTS AND DISCUSSION

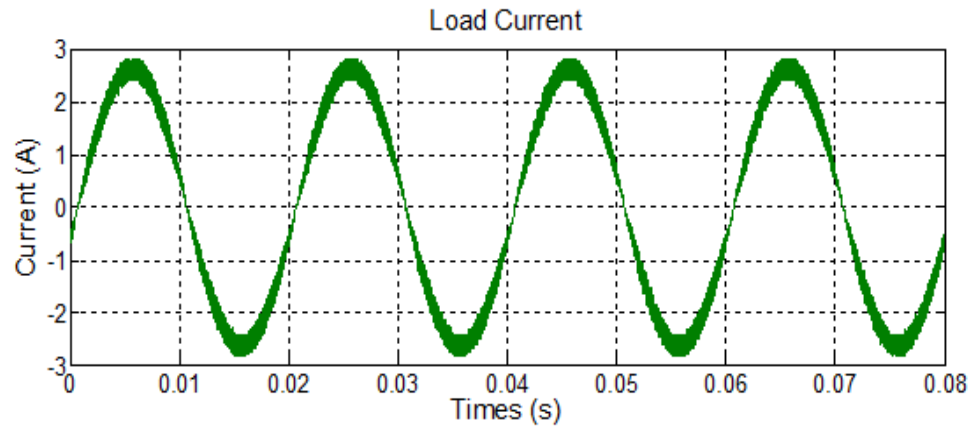
### 4.1 Introduction

This chapter shows the simulation and practical implementation results of closed-loop PI and PR current controller for single-phase inverter. MATLAB/SIMULINK® software is used for the simulation. The performance of both controllers is compared in terms of steady-state response, transient response, current total harmonic distortion (THDi) and also response to frequency variation in the sinusoidal reference signal. The controller parameters obtained from the simulation is used for experimental verification. Simulation and experimental studies are performed on a 250W inverter at 110 V rms. The RMS current is therefore equal to 2.27 A rms with 3.21 A peak.

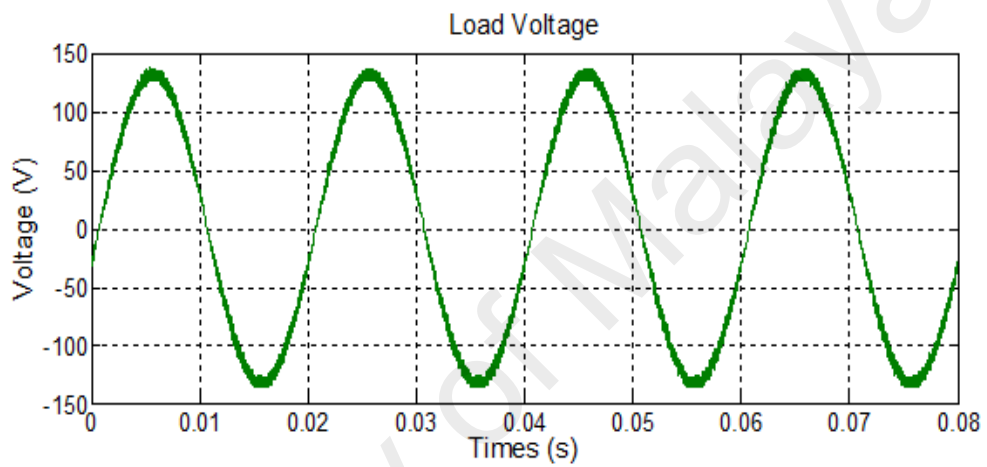
### 4.2 Steady-State Response of PI Controller

The switching frequency of the inverter is set to 20 kHz. The value of  $K_p$  and  $K_i$  for the PI controller are optimally set to 0.5 and 200 respectively. The simulation results of load current, voltage and FFT analysis are presented in Figure 4.1 (a), (b) and (c) respectively. When using PI controller the FFT analysis on the load current yields a THD value equal to 6.43% as shown in Figure 4.1 (c).

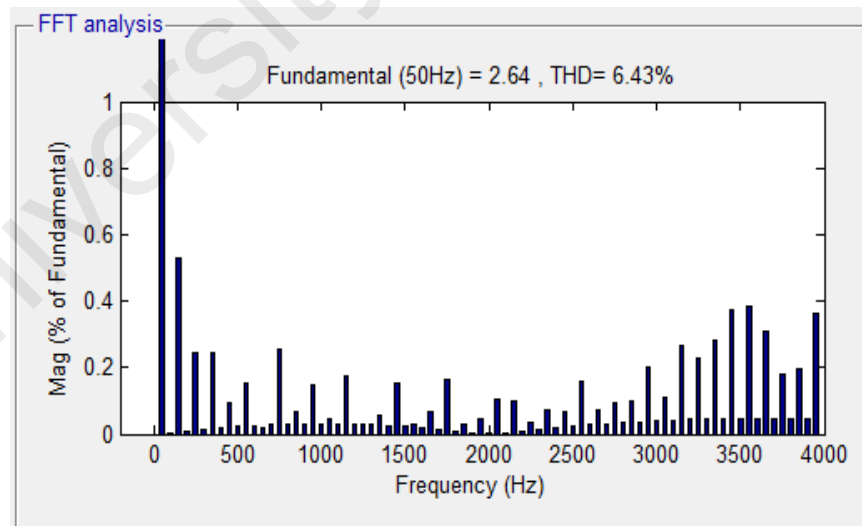
Figure 4.2 show the experimental results of load current and voltage waveforms obtained by using the PI controller. From the figure, the load current reached only 2.8 A peak, in which represents an error of 12.77% from the reference current ( $I_{ref}$ ), 3.21 A peak. Both experiment and simulation results of load current have shown that steady-state error occurred when using PI controller. The FFT analysis showing the current harmonics shown in Figure 4.3, where the percentage of the 3<sup>rd</sup> and 5<sup>th</sup> harmonics were found to be 4.2% and 1.77% respectively.



(a)



(b)



(c)

**Figure 4.1:** Simulation results using PI controller (a) load current, (b) load voltage and (c) FFT analysis



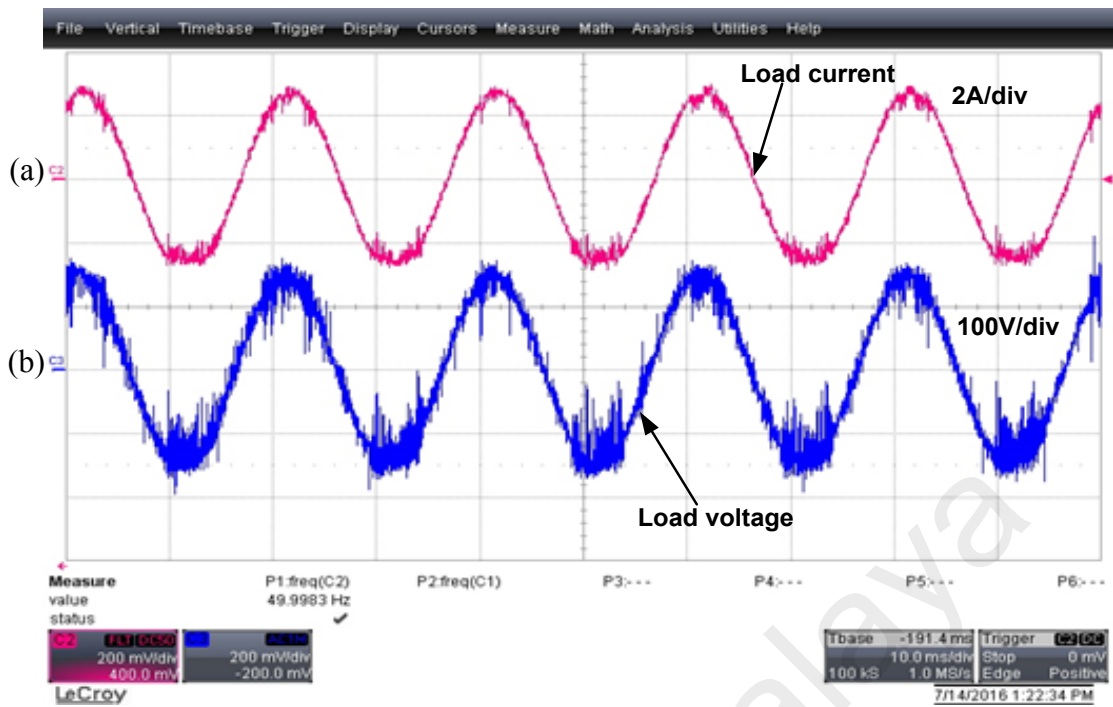


**Figure 4.2:** Experiment results using PI controller ( $K_p = 0.5$  and  $K_i = 200$ ) (a) load current and (b) load voltage

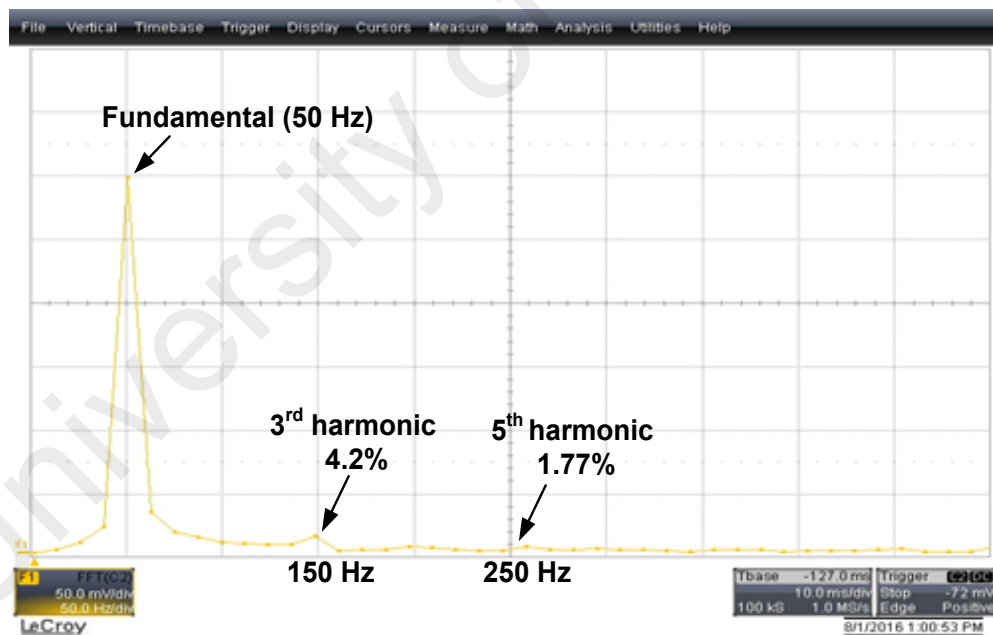


**Figure 4.3:** Experiment result using PI controller showing load current harmonics

When the value of  $K_p$  is increased ( $K_p = 0.7$ ), the results of load current and voltage are shown in Figure 4.4. The current reached the maximum 3.21 A peak, but it is over modulated and therefore increased the 3<sup>rd</sup> harmonic level.

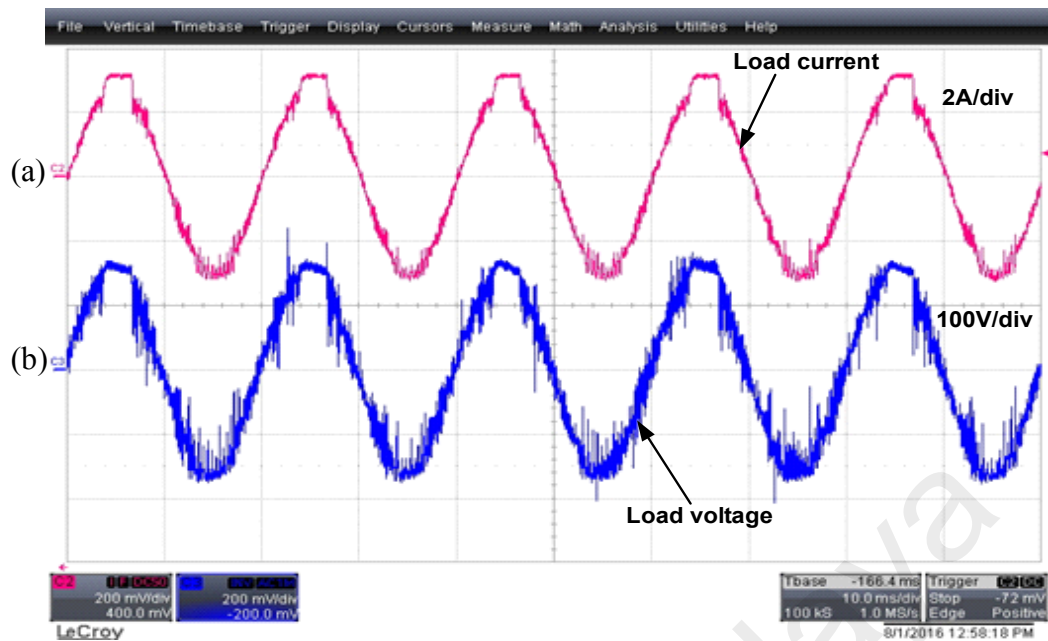


**Figure 4.4:** Experiment results using the PI controller ( $K_p = 0.7$  and  $K_i = 200$ ) (a) load current and (b) load voltage

### 4.3 Steady-State Response of PR Controller

The PR controller parameters,  $K_p$ ,  $K_i$  and  $\omega_c$  are optimally set to 0.5, 1000 and 0.1 rad/s respectively. Simulation results of load current, voltage and FFT analysis are shown in Figure 4.5 (a), (b) and (c) respectively. The THD of the load current is lower when using PR controller where the value is equal to 4.85% as shown Figure 4.5 (c). The simulation results show that PR controller can track the sinusoidal reference current with zero steady-state error and able to suppress current harmonics better than PI controller.

The experimental results of load current and voltage waveforms are shown in Figure 4.6. The load current able to reach the maximum 3.21 A peak of the current reference. It is clear that the load current achieved zero steady-state error as compared to PI controller, 12.77 %. The FFT analysis showing the current THD is given in Figure 4.7, where the magnitude of 3<sup>rd</sup> and 5<sup>th</sup> harmonics were found to be 3.8% and 1.61% respectively.

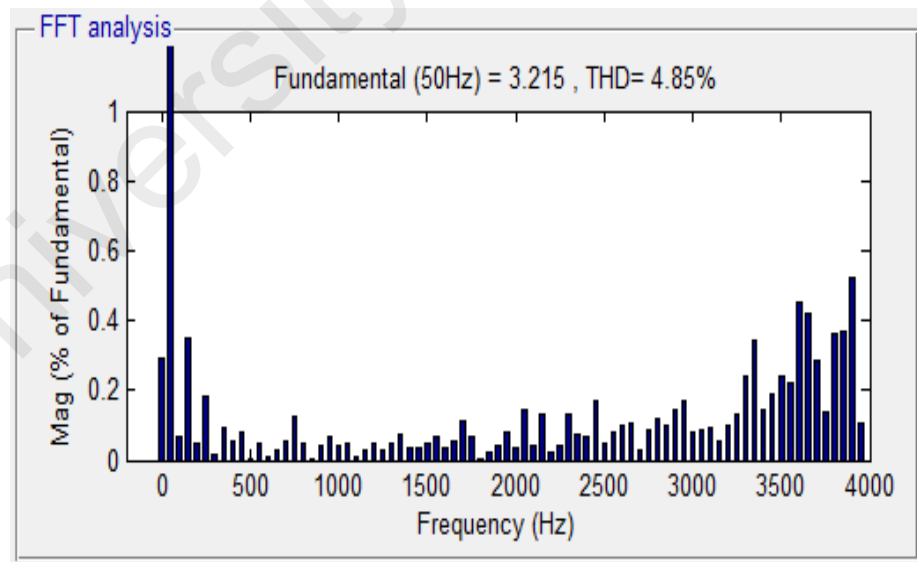
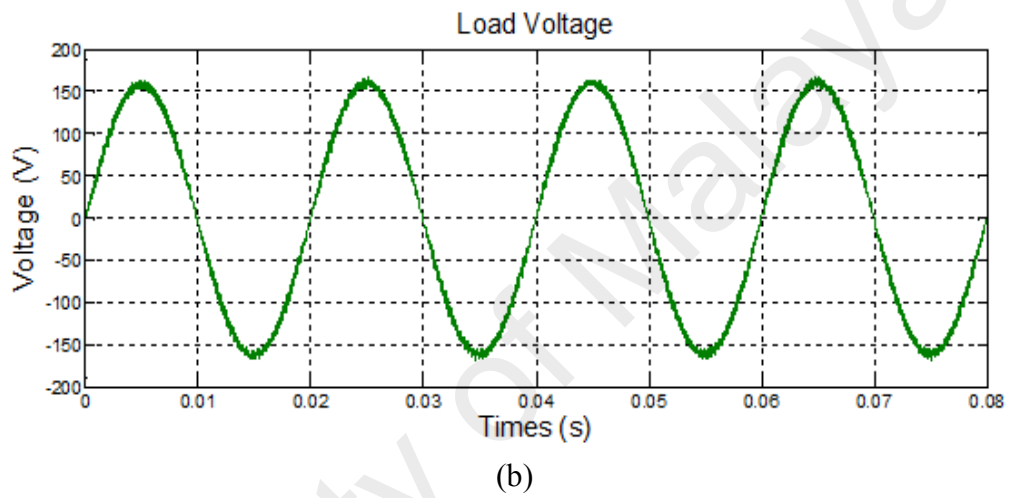
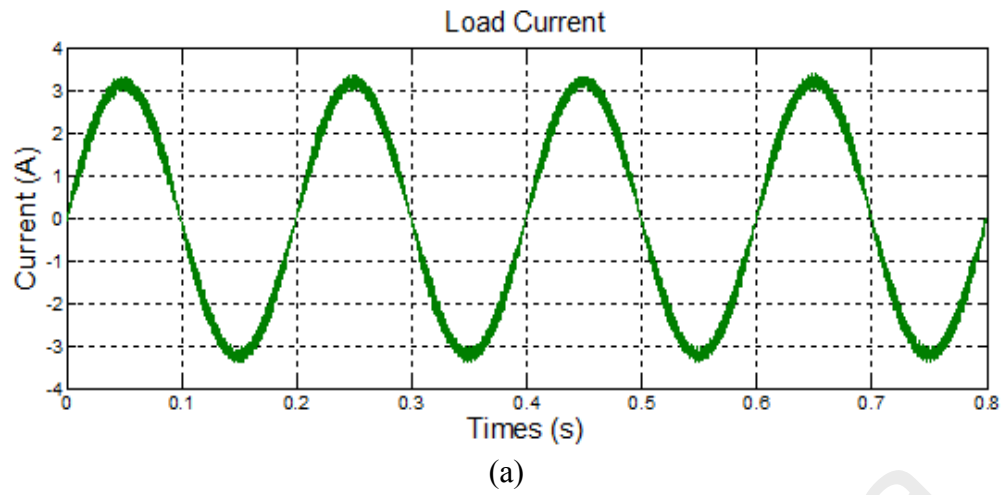


**Figure 4.5:** Simulation results using PR controller (a) load current, (b) load voltage and (c) FFT analysis

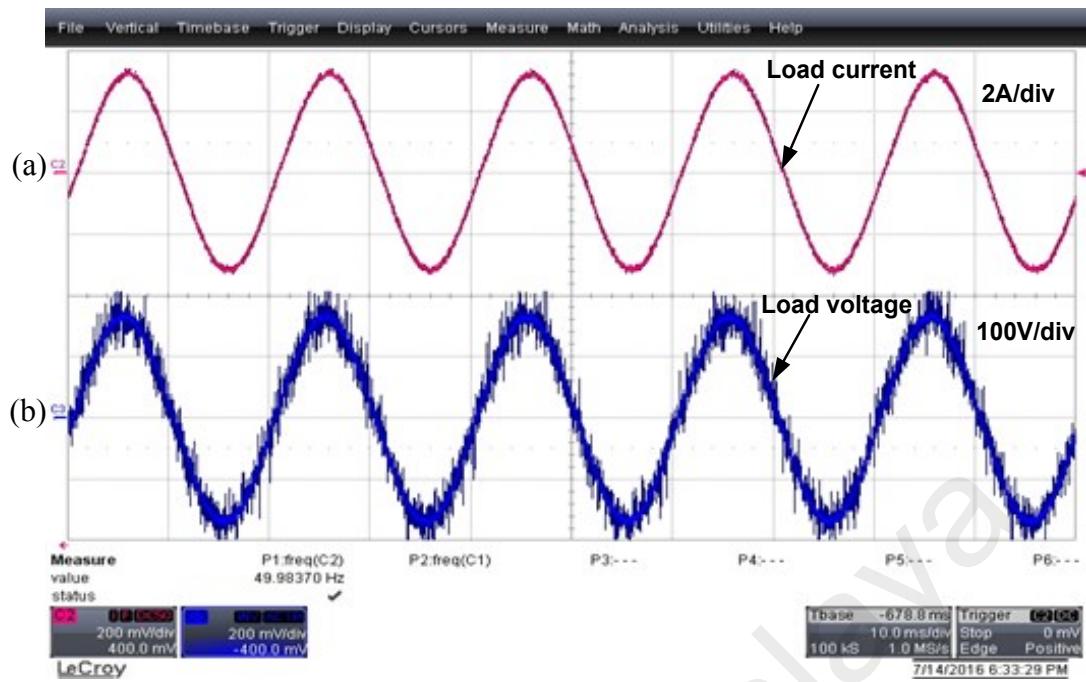


Figure 4.6: Experimental results using PR controller ( $K_p = 0.5$  and  $K_i = 1000$ ) (a) load current (b) load voltage

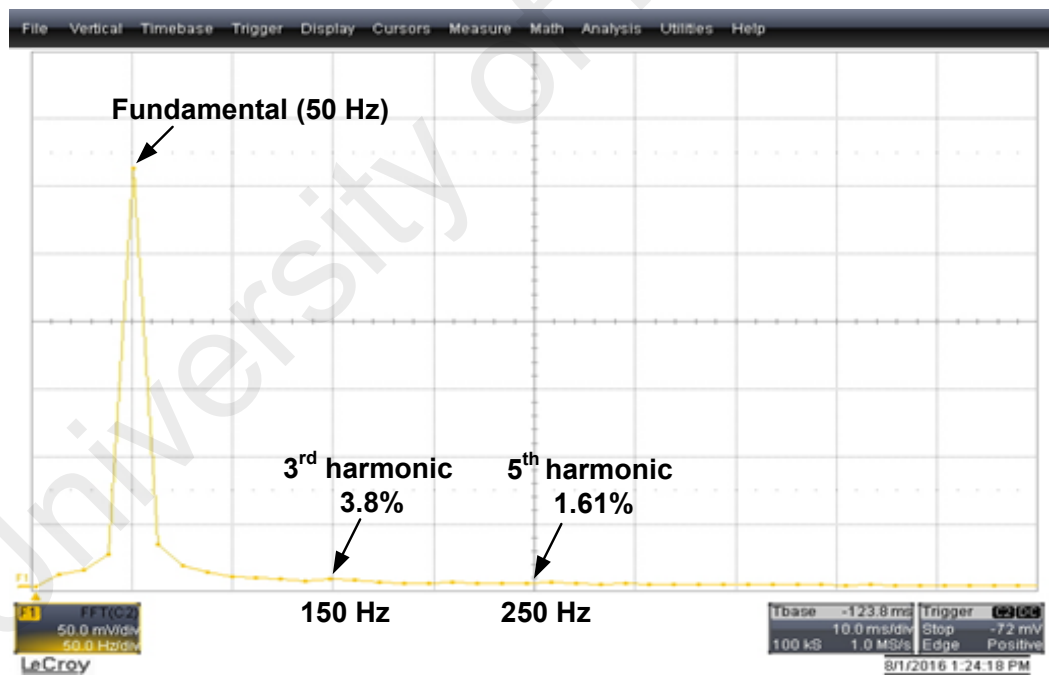
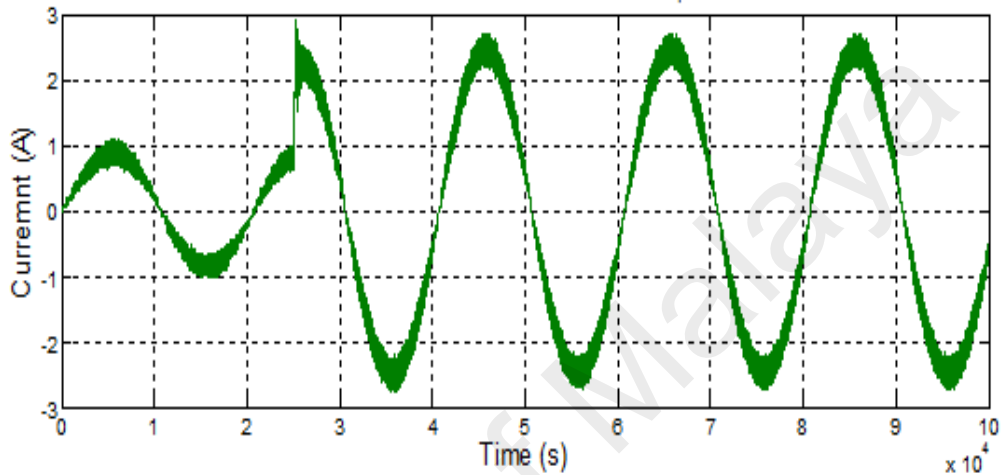


Figure 4.7: Experimental results using PR controller showing load current harmonics

#### 4.4 Transient Response of PI Controller

The transient performance was examined by applying a step change in the current reference during normal conditions. Figure 4.8 depicts the simulation results for the step response in the load current using the PI controller. It can be seen that the PI controller is able to achieve a fast response to reach the steady-state condition.



**Figure 4.8:** Simulation result showing the transient response in load current by using the PI controller

When the value of  $K_p$  is set to 0.5 and  $K_i$  is varied to three different values, 100, 200 and 300. The experimental results of transient response are shown in Figure 4.9, Figure 4.10 and Figure 4.11 respectively. In all conditions, the current reference was changed from 1 A peak to 3.21 A peak. In each case, the results for the load current, controller output response and step signal are shown.

From the analysis of transient response, the PI controller shows a reduced steady-state error when the value of  $K_i$  is increased from 100 to 300 but this leads to over modulation and caused more ripple in the load current.

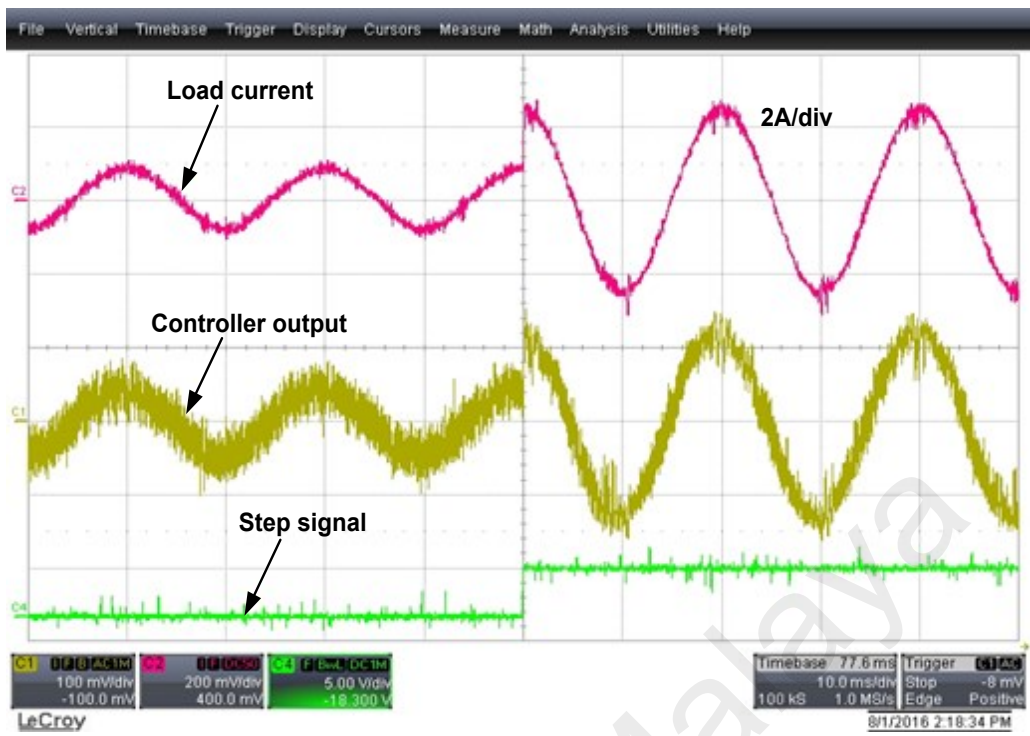


Figure 4.9: Experimental results showing transient response using PI controller for  $K_p = 0.5$ ,  $K_i = 100$

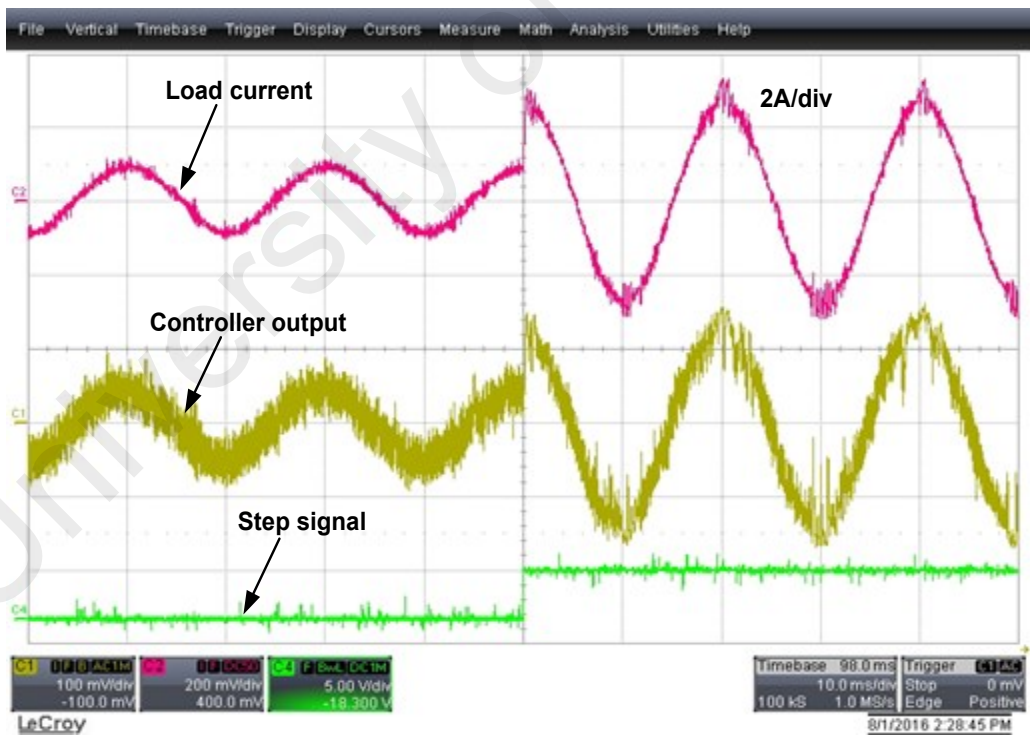
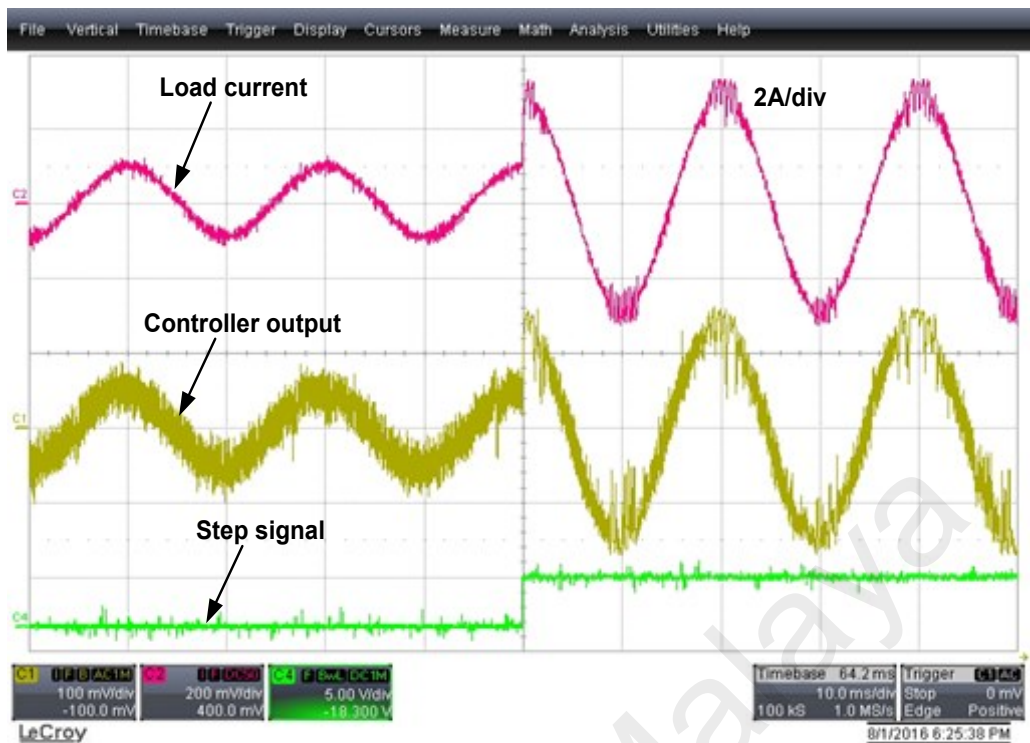


Figure 4.10: Experimental results showing transient response using PI controller for  $K_p = 0.5$ ,  $K_i = 200$



**Figure 4.11:** Experimental results showing transient response using PI controller for  $K_p = 0.5$ ,  $K_i = 300$

#### 4.5 Transient Response of PR Controller

Figure 4.12 shows the simulation results for the step response in the load current using the PR controller. The PR controller shows a fairly fast response and comparable to the PI controller performance.

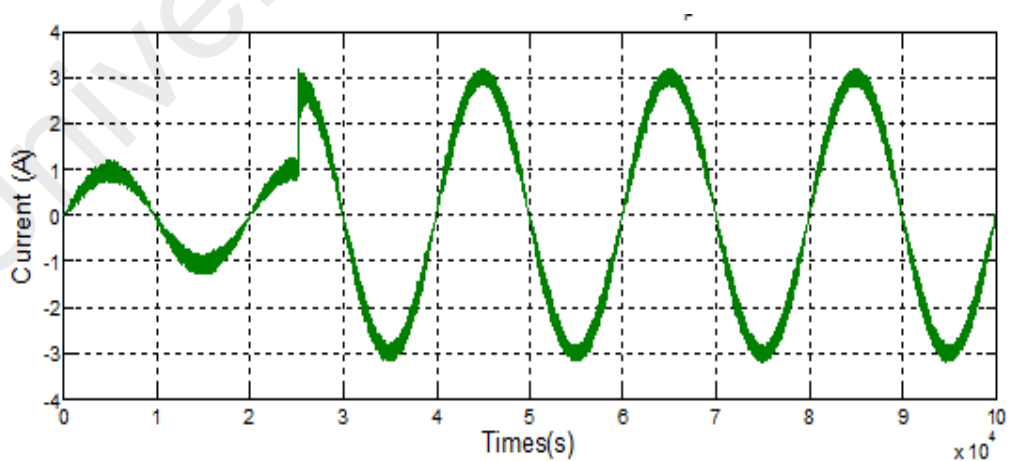


**Figure 4.12:** Simulation result-transient response of load current using by the PR controller.

For experimental verification, the value of  $K_p$  is set to 0.5 while varying the value of  $K_i$  to 1000, 2000 and 3000. The results for the three different controller parameters are shown in Figure 4.13, Figure 4.14 and Figure 4.15 respectively with the current reference stepped from 1 A peak to 3.21 A peak. The transient response of PR controller is slightly slower where it takes a few cycles to reach the steady-state condition. But, it produces higher output quality with very low current harmonics as compared to PI controller with high distortion especially at both positive and negative peak of the load current. This is also reflected by the smooth controller output response in PR as compared to that of PI controller shown in the figures.

For each case, the system is tested under the same value of  $K_p$  and a different value of  $K_i$ . It can be seen from the step response analysis that the controller response is faster when  $K_i$  is increased. Increasing  $K_i$  to a higher value will cause more distortion as more harmonic components around the fundamental frequency are included.

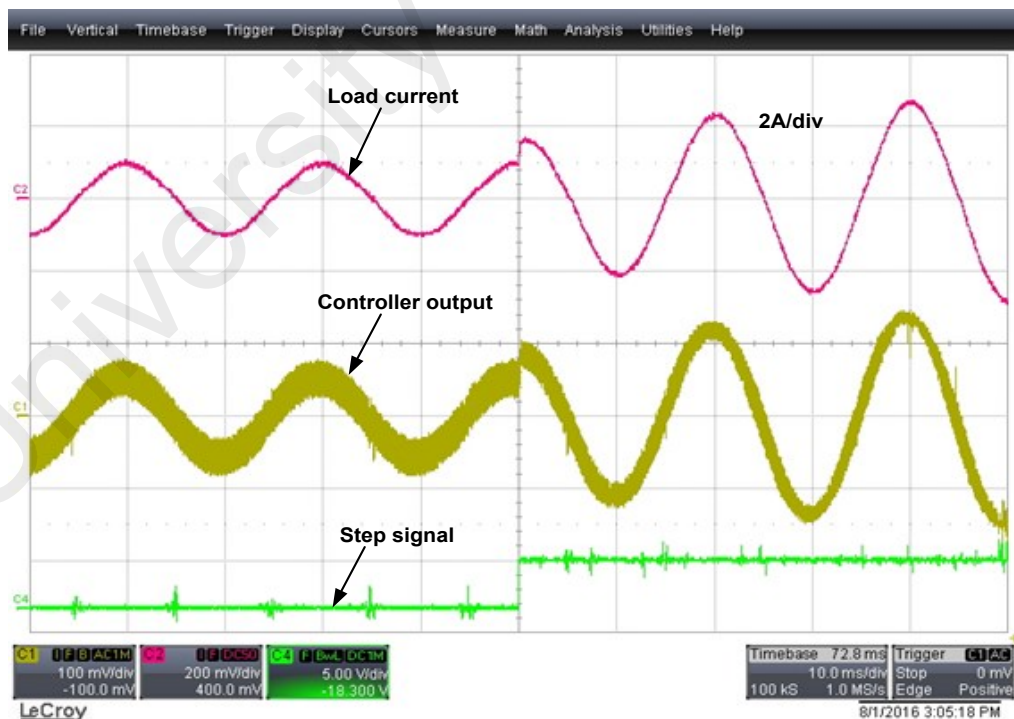


**Figure 4.13:** Experiment results showing transient response using PR controller for  $K_p = 0.5$ ,  $K_i = 1000$



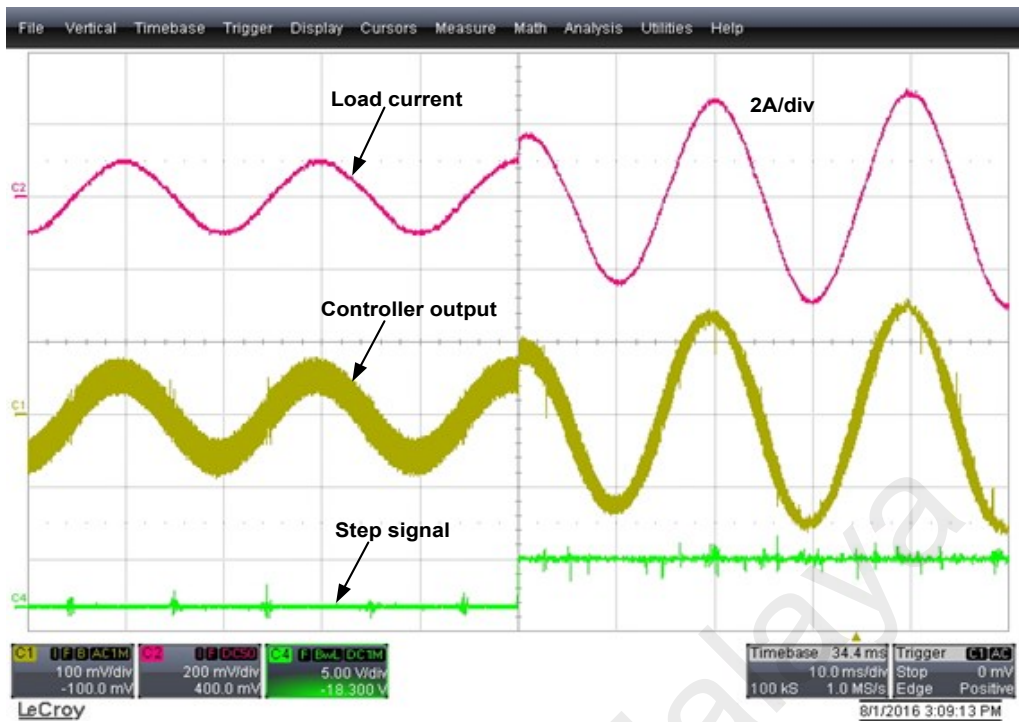


Figure 4.14: Experiment results showing transient response using PR controller for  $K_p = 0.5$ ,  $K_i = 2000$

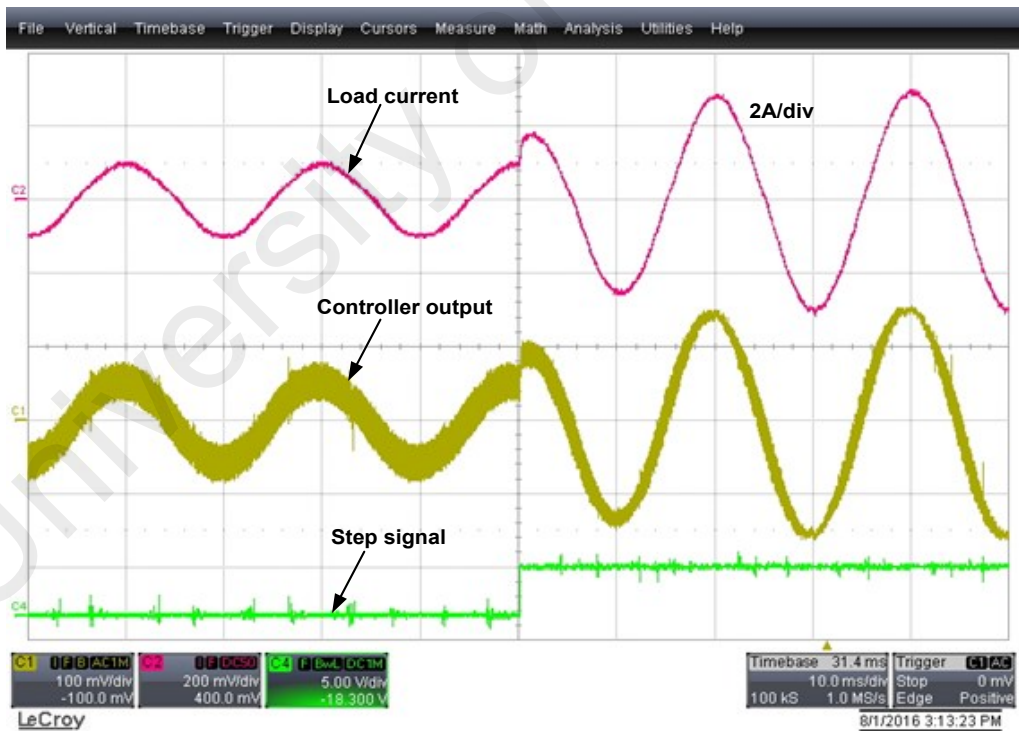
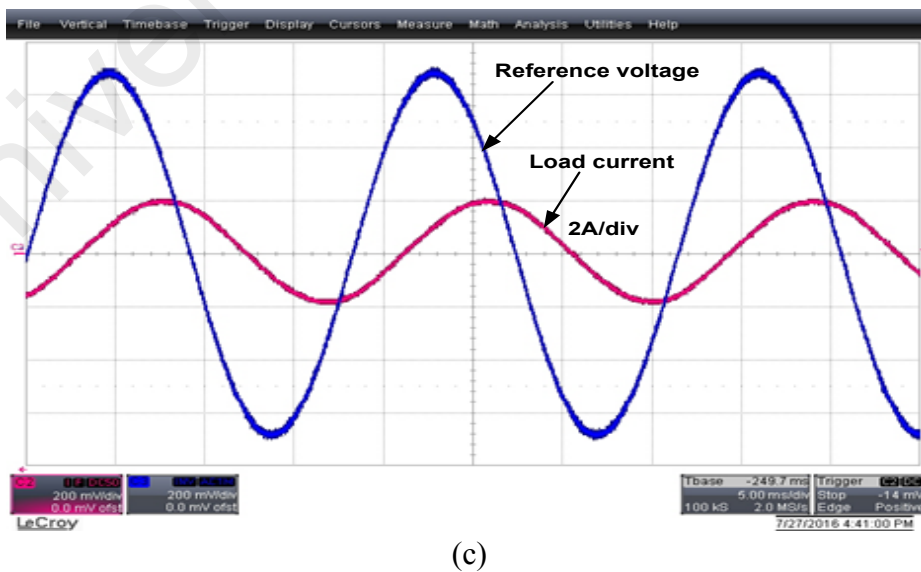
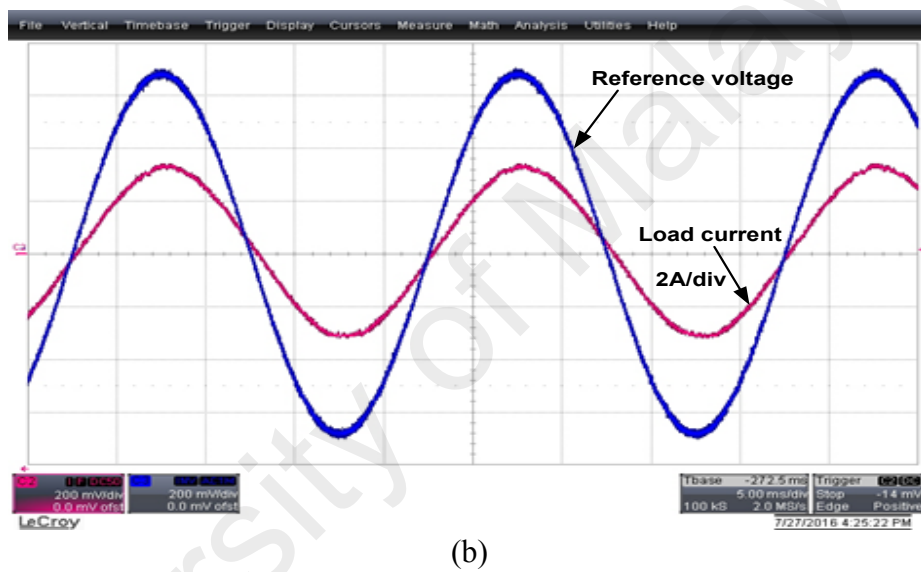
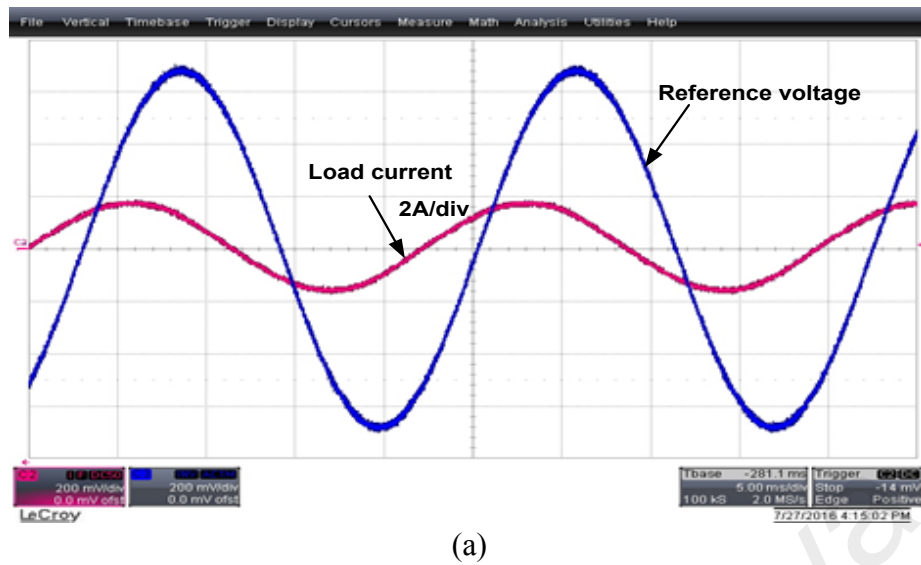


Figure 4.15: Experiment results showing transient response using PR controller for  $K_p = 0.5$ ,  $K_i = 3000$

#### 4.6 Effect of Frequency Variation for PR Controller

Although the PR controller has more advantages as compared to the PI controllers, its performance can be affected by a certain factor such as frequency variation. When the reference signal frequency is different from the fundamental frequency setting of the PR controller, the expected output will be attenuated and contains a phase error. Therefore the effect of frequency variation is investigated when the reference signal frequency is higher and lower than the fundamental frequency. The effect of frequency variation is not performed on PI controller since its output contains magnitude and phase errors even at the fundamental frequency.

Figure 4.16 (a), (b) and (c) show the effect when the frequencies were set to 45 Hz, 50 Hz and 55 Hz respectively. Frequency,  $f = 45$  Hz indicates under frequency whereas  $f = 55$  Hz indicates over frequency. This occurs when the frequency of the reference signal is not the same as the fundamental frequency of the PR controller (50 Hz). Generating reference signal from look-up table will not have this issue, only when the reference signal is externally sourced such as from the grid or other sine-wave generators. When the reference signal frequency is set at  $f = 45$  Hz, the output current is phase-shifted by  $53.91^\circ$  (leading) with respect to the reference voltage as illustrated in Figure 4.16 (a). The current has reached only about 1.8 A peak. The frequency has dropped 10%, and the load current is found to be 43.92% of the current reference. When the system frequency is normal  $f = 50$  Hz, the load current is almost in phase with respect to the reference voltage as shown in Figure 4.16 (b). The load current has reached the maximum current of 3.21 A. When the system frequency is set at  $f = 55$  Hz, the current is phase-shifted by  $60^\circ$  (lagging) and obtained 2 A peak as shown in Figure 4.16 (c). It can be seen from Figure 4.17 (c) that when the system frequency rises by 10% when the load current drops to 37.69%.



**Figure 4.16:** Effect of frequency variation using PR controller (a) under frequency at  $f = 45$  Hz, (b) normal frequency at  $f = 50$  Hz and (c) over frequency at  $f = 55$  Hz)

It has been observed that phase-shift and amplitude change occurs with frequency variation in the reference signal for the practical PR transfer function represented by Equation (2.3). The effects are expected and illustrated by the closed-loop frequency response of the controller in Figure 3.10. The controller gain is finite and relatively high at the fundamental frequency for enforcing a small steady-state error. The controller's bandwidth can be widened by setting  $\omega_c$  appropriately, which helps to reduce sensitivity towards slight frequency variations,  $K_i$  can be tuned for shifting the magnitude response vertically, but this does not give rise to a significant variation in bandwidth (Alexandra et al., 2013; Teodorescu et al., 2006; Teodorescu et al., 2011).

#### 4.7 Summary Comparison of Current Controllers

Good stability, low steady-state error, fast transient response and low harmonics distortion are among the desirable features needed to achieve superior inverter performance. Table 4.1 summarizes the benefits and limitations of PI and PR controllers in various current-controlled applications.

**Table 4.1:** Benefits and limitations of PI and PR current controllers

Controller type	Benefits	Limitations
PI controller	<ul style="list-style-type: none"> <li>• Easy hardware implementation</li> <li>• Simple current control</li> <li>• Good dynamic response</li> </ul>	<ul style="list-style-type: none"> <li>• Very poor harmonics compensation</li> <li>• Steady-state error is not eliminated</li> </ul>
PR controller	<ul style="list-style-type: none"> <li>• High gain around resonance frequency</li> <li>• Very low steady-state error</li> <li>• Good dynamic response</li> <li>• High current harmonic compensation especially low-order harmonics</li> </ul>	<ul style="list-style-type: none"> <li>• Comparatively complex software implementation</li> </ul>

## CHAPTER 5: CONCLUSION AND FUTURE WORK

### 5.1 Conclusion

In this study, the detailed analysis and implementation of PR controller for a single-phase inverter for renewable energy applications has been completed, that include both open-loop and closed-loop analysis. The PR current controller was found to be the most promising controller for single-phase inverter application because it has an infinite gain at the fundamental frequency, which can achieve zero steady-state error and good transient response. The PR controller is advantageous over the well-known PI controller that has significant drawbacks such as steady-state error, phase error, and limited disturbance rejection capability from the comparison that have been made by simulation and experiment. Both controllers have optimally been tuned for fair comparison and implemented using the same inverter prototype and load. For PR controller, the parameters such as  $K_p$ ,  $K_i$  and  $\omega_c$  have optimally been determined by the phase margin analysis using the bode plots. In addition, the effect of frequency variation to the controller performances has also been demonstrated for under, over and normal frequency conditions. The experimental results obtained validate the simulation and analytical analysis that has been carried out on the PR current controller.

### 5.2 Future Work

Several suggestions are provided for future enhancement of this research work. They are listed below in points form.

- Implementing the PR controller for single-phase / three-phase grid-connected PV inverters.
- Developing the new optimization technique to enhance the performance of the PR controller for renewable energy application.

## REFERENCES

- Abdel-Qawee, I., Abdel-Rahim, N., Mansour, H. A., & Dakrory, T. (2013, Aug. 31 2013-Sept. 2 2013). *Closed-loop control of single phase selective harmonic elimination PWM inverter using proportional-resonant controller*. Paper presented at the Modelling, Identification & Control (ICMIC), 2013 Proceedings of International Conference on.
- Agirman, I., & Blasko, V. (2003). A novel control method of a VSC without AC line voltage sensors. *Industry Applications, IEEE Transactions on*, 39(2), 519-524. doi: 10.1109/TIA.2003.808925
- Alepuz, S., Busquets-Monge, S., Bordonau, J., Gago, J., Gonzalez, D., & Balcells, J. (2006). Interfacing Renewable Energy Sources to the Utility Grid Using a Three-Level Inverter. *Industrial Electronics, IEEE Transactions on*, 53(5), 1504-1511. doi: 10.1109/TIE.2006.882021
- Alexandra, C., Almaktoof, A. M., & Raji, A. (2013). Development of a proportional+ resonant (PR) controller for a three-phase AC micro-grid system.
- Basic, D., Ramsden, V. S., & Mutik, P. K. (2001). Harmonic filtering of high-power 12-pulse rectifier loads with a selective hybrid filter system. *IEEE Transactions on Industrial Electronics*, 48(6), 1118-1127. doi: 10.1109/41.969390
- Bin, Y., & Liuchen, C. (2005, 16-16 June 2005). *Improved Predictive Current Controlled PWM for Single-Phase Grid-Connected Voltage Source Inverters*. Paper presented at the Power Electronics Specialists Conference, 2005. PESC '05. IEEE 36th.
- Bin, Z., Danwei, W., Keliang, Z., & Yigang, W. (2008). Linear Phase Lead Compensation Repetitive Control of a CVCF PWM Inverter. *Industrial Electronics, IEEE Transactions on*, 55(4), 1595-1602. doi: 10.1109/TIE.2008.917105
- Blaabjerg, F., Teodorescu, R., Liserre, M., & Timbus, A. V. (2006). Overview of Control and Grid Synchronization for Distributed Power Generation Systems. *Industrial Electronics, IEEE Transactions on*, 53(5), 1398-1409. doi: 10.1109/TIE.2006.881997
- Bode, G. H., Poh Chiang, L., Newman, M. J., & Holmes, D. G. (2005). An improved robust predictive current regulation algorithm. *Industry Applications, IEEE Transactions on*, 41(6), 1720-1733. doi: 10.1109/TIA.2005.858324
- Bojoi, R., Limongi, L. R., Ruiu, D., & Tenconi, A. (2008, 10-13 Nov. 2008). *Frequency-domain analysis of resonant current controllers for active power conditioners*. Paper presented at the Industrial Electronics, 2008. IECON 2008. 34th Annual Conference of IEEE.
- Buso, S., Fasolo, S., Malesani, L., & Mattavelli, P. (1999, 1999). *A dead-beat adaptive hysteresis current control*. Paper presented at the Industry Applications

Conference, 1999. Thirty-Fourth IAS Annual Meeting. Conference Record of the 1999 IEEE.

- Buso, S., Malesani, L., & Mattavelli, P. (1998). Comparison of current control techniques for active filter applications. *Industrial Electronics, IEEE Transactions on*, 45(5), 722-729. doi: 10.1109/41.720328
- Camacho, E. F., Rubio, F. R., Berenguel, M., & Valenzuela, L. (2007). A survey on control schemes for distributed solar collector fields. Part II: Advanced control approaches. *Solar Energy*, 81(10), 1252-1272. doi: <http://dx.doi.org/10.1016/j.solener.2007.01.001>
- Cao, Y. (2014). Theory and performance analysis of a new heat engine for concentrating solar power. *International Journal of Energy Research*, 38(14), 1812-1824. doi: 10.1002/er.3187
- Castilla, M., Miret, J., Matas, J., Vicuna, L. G. d., & Guerrero, J. M. (2009). Control Design Guidelines for Single-Phase Grid-Connected Photovoltaic Inverters With Damped Resonant Harmonic Compensators. *IEEE Transactions on Industrial Electronics*, 56(11), 4492-4501. doi: 10.1109/TIE.2009.2017820
- Chen, J. F., Chu, C. L., & Huang, C. L. (1992, 25-29 May 1992). *The parallel operation of two UPS by the coupled-inductor method*. Paper presented at the Industrial Electronics, 1992., Proceedings of the IEEE International Symposium on.
- Chiang, S. J., Liaw, C. M., Chang, W. C., & Chang, W. Y. (1996). Multi-module parallel small battery energy storage system. *IEEE Transactions on Energy Conversion*, 11(1), 146-154. doi: 10.1109/60.486589
- Chung, S. K. (2000). Phase-locked loop for grid-connected three-phase power conversion systems. *Electric Power Applications, IEE Proceedings -*, 147(3), 213-219. doi: 10.1049/ip-epa:20000328
- Cortes, P., Kazmierkowski, M. P., Kennel, R. M., Quevedo, D. E., & Rodriguez, J. (2008). Predictive Control in Power Electronics and Drives. *Industrial Electronics, IEEE Transactions on*, 55(12), 4312-4324. doi: 10.1109/TIE.2008.2007480
- Costa, C., x, R., Grino, R., & Fossas, E. (2004). Odd-harmonic digital repetitive control of a single-phase current active filter. *Power Electronics, IEEE Transactions on*, 19(4), 1060-1068. doi: 10.1109/TPEL.2004.830045
- de la Parra, I., Marcos, J., García, M., & Marroyo, L. (2015). Control strategies to use the minimum energy storage requirement for PV power ramp-rate control. *Solar Energy*, 111, 332-343. doi: <http://dx.doi.org/10.1016/j.solener.2014.10.038>
- Du, D., Darkwa, J., & Kokogiannakis, G. (2013). Thermal management systems for Photovoltaics (PV) installations: A critical review. *Solar Energy*, 97, 238-254. doi: <http://dx.doi.org/10.1016/j.solener.2013.08.018>

- Espinoza, K., Valera, D., Torres, J., López, A., & Molina-Aiz, F. (2015). An Auto-Tuning PI Control System for an Open-Circuit Low-Speed Wind Tunnel Designed for Greenhouse Technology. *Sensors*, 15(8), 19723.
- Fukuda, S., & Yoda, T. (2001). A novel current-tracking method for active filters based on a sinusoidal internal model [for PWM invertors]. *Industry Applications, IEEE Transactions on*, 37(3), 888-895. doi: 10.1109/28.924772
- Gabe, I. J., Montagner, V. F., & Pinheiro, H. (2009). Design and implementation of a robust current controller for VSI connected to the grid through an LCL filter. *IEEE Transactions on Power Electronics*, 24(6), 1444-1452.
- Gálvez-Carrillo, M., De Keyser, R., & Ionescu, C. (2009). Nonlinear predictive control with dead-time compensator: Application to a solar power plant. *Solar Energy*, 83(5), 743-752. doi: <http://dx.doi.org/10.1016/j.solener.2008.11.005>
- Guo, X., Zhao, Q., & Wu, W. (2006, 14-16 Aug. 2006). *A Single-Phase Grid-Connected Inverter System With Zero Steady-State Error*. Paper presented at the Power Electronics and Motion Control Conference, 2006. IPERC 2006. CES/IEEE 5th International.
- Hanju, C., Trung-Kien, V., & Jae-Eon, K. (2009, 20-24 Sept. 2009). *Design and control of Proportional-Resonant controller based Photovoltaic power conditioning system*. Paper presented at the Energy Conversion Congress and Exposition, 2009. ECCE 2009. IEEE.
- Hasanuzzaman, M., Rahim, N. A., Hosenuzzaman, M., Saidur, R., Mahbubul, I. M., & Rashid, M. M. (2012). Energy savings in the combustion based process heating in industrial sector. *Renewable and Sustainable Energy Reviews*, 16(7), 4527-4536. doi: <http://dx.doi.org/10.1016/j.rser.2012.05.027>
- Hasanuzzaman, M., Rahim, N. A., Saidur, R., & Kazi, S. N. (2011). Energy savings and emissions reductions for rewinding and replacement of industrial motor. *Energy*, 36(1), 233-240. doi: <http://dx.doi.org/10.1016/j.energy.2010.10.046>
- Hassaine, L., Olias, E., Quintero, J., & Salas, V. (2014). Overview of power inverter topologies and control structures for grid connected photovoltaic systems. *Renewable and Sustainable Energy Reviews*, 30, 796-807. doi: <http://dx.doi.org/10.1016/j.rser.2013.11.005>
- Hobraiche, J., Vilain, J. P., Macret, P., & Patin, N. (2009). A New PWM Strategy to Reduce the Inverter Input Current Ripples. *IEEE Transactions on Power Electronics*, 24(1), 172-180. doi: 10.1109/TPEL.2008.2006357
- Hojabri, M., Ahmad, A. Z., Toudeshki, A., & Soheilrad, M. (2012). An overview on current control techniques for grid connected renewable energy systems. *International Proceedings of Computer Science and Information Technology*, 56, 119.
- Hosseini, S. E., & Abdul Wahid, M. (2014). The role of renewable and sustainable energy in the energy mix of Malaysia: a review. *International Journal of Energy Research*, 38(14), 1769-1792. doi: 10.1002/er.3190



- Huibin, Z., Arnet, B., Haines, L., Shaffer, E., & Jih-Sheng, L. (2003, 9-13 Feb. 2003). *Grid synchronization control without AC voltage sensors*. Paper presented at the Applied Power Electronics Conference and Exposition, 2003. APEC '03. Eighteenth Annual IEEE.
- IEA. (Global Energy Trends, 2014). Renewable energy outlook.
- Islam, M. A., Hasanuzzaman, M., Rahim, N. A., Nahar, A., & Hosenuzzaman, M. (2014). Global Renewable Energy-Based Electricity Generation and Smart Grid System for Energy Security. *The Scientific World Journal*, 2014, 13. doi: 10.1155/2014/197136
- Ito, Y., & Kawauchi, S. (1995). Microprocessor based robust digital control for UPS with three-phase PWM inverter. *Power Electronics, IEEE Transactions on*, 10(2), 196-204. doi: 10.1109/63.372604
- Kazmierkowski, M. P., & Malesani, L. (1998). Current control techniques for three-phase voltage-source PWM converters: a survey. *Industrial Electronics, IEEE Transactions on*, 45(5), 691-703. doi: 10.1109/41.720325
- Keliang, Z., Danwei, W., Bin, Z., & Yigang, W. (2009). Plug-In Dual-Mode-Structure Repetitive Controller for CVCF PWM Inverters. *Industrial Electronics, IEEE Transactions on*, 56(3), 784-791. doi: 10.1109/TIE.2008.2005149
- Keliang, Z., Kay-Soon, L., Yigang, W., Fang-Lin, L., Bin, Z., & Yigang, W. (2006). Zero-phase odd-harmonic repetitive controller for a single-phase PWM inverter. *Power Electronics, IEEE Transactions on*, 21(1), 193-201. doi: 10.1109/TPEL.2005.861190
- Khairy, A., Ibrahim, M., Abdel-Rahim, N., & Elsherif, H. (2011, 6-8 Sept. 2011). *Comparing proportional-resonant and fuzzy-logic controllers for current controlled single-phase grid-connected PWM DC/AC inverters*. Paper presented at the Renewable Power Generation (RPG 2011), IET Conference on.
- Kim, H., & Sul, S.-K. (2005). Compensation voltage control in dynamic voltage restorers by use of feed forward and state feedback scheme. *IEEE Transactions on Power Electronics*, 20(5), 1169-1177.
- Kim, H., & Sul, S. (January 2011). A Novel Filter Design for Output LC Filters of PWM Inverters. *Journal of Power Electronics*, 11(1).
- Kim, H., Yu, T., & Choi, S. (2008). Indirect current control algorithm for utility interactive inverters in distributed generation systems. *IEEE Transactions on Power Electronics*, 23(3), 1342-1347.
- Kim, Y.-S., Chung, I.-Y., & Moon, S.-I. (2015). Tuning of the PI Controller Parameters of a PMSG Wind Turbine to Improve Control Performance under Various Wind Speeds. *Energies*, 8(2), 1406.
- Lee, J. H., Hae-Gwang Jeong, H.G., and Lee, K.B., . (2012). Performance Improvement of Grid-Connected Inverter Systems under Unbalanced and Distorted Grid Voltage by Using a PR Controller. *JEET*, 7(6), 918-925. doi: 10.5370

- Lezana, P., Silva, C. A., Rodriguez, J., & Perez, M. A. (2007). Zero-Steady-State-Error Input-Current Controller for Regenerative Multilevel Converters Based on Single-Phase Cells. *Industrial Electronics, IEEE Transactions on*, 54(2), 733-740. doi: 10.1109/TIE.2007.891994
- Liserre, M., Blaabjerg, F., & Teodorescu, R. (2005). *Grid impedance detection via excitation of LCL-filter resonance*. Paper presented at the Fourtieth IAS Annual Meeting. Conference Record of the 2005 Industry Applications Conference, 2005.
- Mattavelli, P., Spiazzi, G., & Tenti, P. (2003, 15-19 June 2003). *Predictive digital control of power factor preregulators using disturbance observer for input voltage estimation*. Paper presented at the Power Electronics Specialist Conference, 2003. PESC '03. 2003 IEEE 34th Annual.
- Mattavelli, P., Spiazzi, G., & Tenti, P. (2005). Predictive digital control of power factor preregulators with input voltage estimation using disturbance observers. *Power Electronics, IEEE Transactions on*, 20(1), 140-147. doi: 10.1109/TPEL.2004.839821
- Monfared , M., & Golestan , S. (2012). Control strategies for single-phase grid integration of small-scale renewable energy sources: A review. *Renewable and Sustainable Energy Reviews*, 16, 4982–4993.
- Negroni, J. J., Meza, C., Biel, D., & Guinjoan, F. (2005, 20-23 June 2005). *Control of a buck inverter for grid-connected PV systems: a digital and sliding mode control approach*. Paper presented at the Industrial Electronics, 2005. ISIE 2005. Proceedings of the IEEE International Symposium on.
- Newman, M. J., Zmood, D. N., & Holmes, D. G. (2002). Stationary frame harmonic reference generation for active filter systems. *Industry Applications, IEEE Transactions on*, 38(6), 1591-1599. doi: 10.1109/TIA.2002.804739
- Park, S.-Y., Chen, C.-L., Lai, J.-S., & Moon, S.-R. (2008). Admittance compensation in current loop control for a grid-tie LCL fuel cell inverter. *IEEE Transactions on Power Electronics*, 23(4), 1716-1723.
- Pitalúa-Díaz, N., Herrera-López, E., Valencia-Palomo, G., González-Angeles, A., Rodríguez-Carvajal, R., & Cazarez-Castro, N. (2015). Comparative Analysis between Conventional PI and Fuzzy LogicPI Controllers for Indoor Benzene Concentrations. *Sustainability*, 7(5), 5398.
- Saccomando, G., & Svensson, J. (2001, Sept. 30 2001-Oct. 4 2001). *Transient operation of grid-connected voltage source converter under unbalanced voltage conditions*. Paper presented at the Industry Applications Conference, 2001. Thirty-Sixth IAS Annual Meeting. Conference Record of the 2001 IEEE.
- Shukla, A., Ghosh, A., & Joshi, A. (2008). Improved Multilevel Hysteresis Current Regulation and Capacitor Voltage Balancing Schemes for Flying Capacitor Multilevel Inverter. *Power Electronics, IEEE Transactions on*, 23(2), 518-529. doi: 10.1109/TPEL.2007.915788

- Tajuddin, M. F. N., Arif, M. S., Ayob, S. M., & Salam, Z. (2015). Perturbative methods for maximum power point tracking (MPPT) of photovoltaic (PV) systems: a review. *International Journal of Energy Research*, 39(9), 1153-1178. doi: 10.1002/er.3289
- Teodorescu, R., & Blaabjerg, F. (2004). Flexible control of small wind turbines with grid failure detection operating in stand-alone and grid-connected mode. *Power Electronics, IEEE Transactions on*, 19(5), 1323-1332. doi: 10.1109/TPEL.2004.833452
- Teodorescu, R., Blaabjerg, F., Borup, U., & Liserre, M. (2004, 2004). *A new control structure for grid-connected LCL PV inverters with zero steady-state error and selective harmonic compensation*. Paper presented at the Applied Power Electronics Conference and Exposition, 2004. APEC '04. Nineteenth Annual IEEE.
- Teodorescu, R., Blaabjerg, F., Liserre, M., & Loh, P. C. (2006). Proportional-resonant controllers and filters for grid-connected voltage-source converters. *Electric Power Applications, IEE Proceedings*, 153(5), 750-762.
- Teodorescu, R., Iov, F., & Blaabjerg, F. (2003, 15-19 June 2003). *Flexible development and test system for 11 kW wind turbine*. Paper presented at the Power Electronics Specialist Conference, 2003. PESC '03. 2003 IEEE 34th Annual.
- Teodorescu, R., Liserre, M., & Rodriguez, P. (2011). *Grid Converters for Photovoltaic and Wind Power Systems*. Wiley.
- Timbus, A., Liserre, M., Teodorescu, R., Rodriguez, P., & Blaabjerg, F. (2009). Evaluation of Current Controllers for Distributed Power Generation Systems. *Power Electronics, IEEE Transactions on*, 24(3), 654-664. doi: 10.1109/TPEL.2009.2012527
- Twining, E., & Holmes, D. G. (2002, 2002). *Grid current regulation of a three-phase voltage source inverter with an LCL input filter*. Paper presented at the Power Electronics Specialists Conference, 2002. pesc 02. 2002 IEEE 33rd Annual.
- Ünal, A. N., Ercan, S., & Kayakutlu, G. (2015). Optimisation studies on tri-generation: a review. *International Journal of Energy Research*, 39(10), 1311-1334. doi: 10.1002/er.3342
- Wang, D., Yu, P., Wang, F., Chan, H.-Y., Zhou, L., Dong, Z., . . . Li, W. (2015). Improving Atomic Force Microscopy Imaging by a Direct Inverse Asymmetric PI Hysteresis Model. *Sensors*, 15(2), 3409.
- Yang, W.-J., Kuo, C.-H., & Aydin, O. (2001). A hybrid power generation system: solar-driven Rankine engine-hydrogen storage. *International Journal of Energy Research*, 25(12), 1107-1125. doi: 10.1002/er.744
- Yongheng, Y., Keliang, Z., & Blaabjerg, F. (2013, 17-21 March 2013). *Harmonics suppression for single-phase grid-connected PV systems in different operation modes*. Paper presented at the Applied Power Electronics Conference and Exposition (APEC), 2013 Twenty-Eighth Annual IEEE.

- Yu, B., Matsui, M., & Yu, G. (2010). A review of current anti-islanding methods for photovoltaic power system. *Solar Energy*, 84(5), 745-754. doi: <http://dx.doi.org/10.1016/j.solener.2010.01.018>
- Yuan , X., Merk ,W.,Stemmler ,H.,and Allmeling ,J.,. (2002). Stationary-Frame Generalized Integrators for Current Control of Active Power Filters with Zero steady-state Error for Current Harmonics of Concern Under Unbalanced and Distorted Operating Conditions. *IEEE*, 38(2), 523-532.
- Zammit , D., Staines ,C.S.,and Apap ,M . (2014). Comparison between PI and PR Current Controllers in Grid Connected PV Inverters. *International Journal of Electrical, Electronic Science and Engineering*, 8(2).
- Zmood, D. N., & Holmes, D. G. (2003). Stationary frame current regulation of PWM inverters with zero steady-state error. *Power Electronics, IEEE Transactions on*, 18(3), 814-822. doi: 10.1109/TPEL.2003.810852

University of Malaya

## LIST OF PUBLICATIONS

### Journal paper

- ❖ Parvez, M., Elias, M. F. M., Rahim, N. A., & Osman, N. (2016). Current control techniques for three-phase grid interconnection of renewable power generation systems: A review. *Solar Energy*, 135, 29-42. (Q1, IF: 3.59).
- ❖ Parvez, M., Elias, M. F. M., Rahim, N. A. “Analysis the current harmonic compensation control with effect of frequency variation for single phase stand-alone PV inverters” *IETE Journal of Research* (Under Review).
- ❖ Parvez, M., Elias, M. F. M., Rahim, N. A. “Comparative Study of Proportional-Integral (PI) and Proportional-Resonant (PR) Current Controller for Single-Phase Standalone PV Inverters” *Journal of Renewable and Sustainable Energy* (Under Review).

### Conference paper

- ❖ Parvez, M., Elias, M. F. M., & Rahim, N. A. Performance analysis of PR current controller for single-phase inverters, 2016 4<sup>th</sup> IET International Conference on Clean Energy and Technology (CEAT), 14-15 November, Kuala Lumpur, Malaysia.